Analytical yield criterion for an anisotropic material containing spherical voids and exhibiting tension–compression asymmetry

Joel B. Stewart [a], Oana Cazacu [b,*]

[a] Air Force Research Laboratory, Munitions Directorate, Eglin AFB, FL 32542, United States
[b] Department of Mechanical and Aerospace Engineering, University of Florida REEF, 1350 N Poquito Road, Shalimar, FL 32539, United States

ARTICLE INFO

ABSTRACT

A significant difference between the behavior in tension versus compression is obtained at the polycrystal level if either twinning or non-Schmid effects are contributors to the plastic deformation at the single crystal level. Examples of materials that exhibit tension–compression asymmetry include hexagonal close-packed (HCP) polycrystals and intermetallics (e.g., molybdenum compounds). Despite recent progress in modeling their yield behavior in the absence of voids, the description of coupling between plasticity and damage by void growth in these materials remains a challenge.

This paper is devoted to the development of a macroscopic anisotropic yield criterion for a porous material when the matrix material is incompressible, anisotropic and displays tension–compression asymmetry. The analytical yield criterion is obtained based on micromechanical considerations and non-linear homogenization. The matrix plastic behavior is described by the Cazacu et al. (2006) anisotropic yield criterion that is pressure-insensitive and accounts for strength–differential effects. Comparison between finite element cell calculations and theory show the predictive capabilities of the developed anisotropic model in terms of modeling the combined effects of anisotropy, tension–compression asymmetry of the matrix and voids on the overall yielding of the porous aggregate. It is shown that if the matrix material does not display tension–compression asymmetry, the developed criterion reduces to that of Benzerga and Besson (2001). If the matrix is isotropic, it reduces to the isotropic criterion developed in Cazacu and Stewart (2009).

© 2010 Elsevier Ltd. All rights reserved.

1. Introduction

Ductile failure in metals occurs due to the nucleation, growth and coalescence of voids (McClintock, 1968; Rousselier, 1987). Voids are nucleated in metals mainly by decohesion at the particle–matrix interfaces or by micro-cracking of second-phase particles (see, for example, Tvergaard, 1981). Additionally, voids can nucleate in single crystals that contain neither pre-existing voids nor inclusions (see, for example, Cuitiño and Ortiz, 1996; Lubarda et al., 2004 and the recent studies on cylindrical void growth in rigid-ideally plastic single crystals of Kysar et al., 2005, 2006; Kysar and Gan, 2007). Thus, the ability to accurately describe the evolution of voids in a ductile metal is crucial to being able to accurately predict its failure.

Gurson (1977) developed widely used macroscopic yield criteria for porous metals containing either spherical or cylindrical voids and with the matrix obeying the von Mises isotropic yield condition. The success of Gurson's (1977) criterion lies in the fact that it was deduced based on micromechanical considerations. Several modifications of Gurson's (1977) criterion were proposed (see Tvergaard, 1981; Tvergaard and Needleman, 1984; Koplik and Needleman, 1988) based on finite element calculations to account for void interaction and coalescence. Gologanu et al. (1993, 1994, 1997) generalized Gurson's (1977) analysis by considering a spheroidal volume containing a confocal spheroidal cavity. In Garajeu (1995) and Garajeu et al. (2000) the overall response of a porous metal with a viscous matrix was investigated. Gurson's analysis has also been extended to the case when the matrix material is compressible and obeys a Drucker-Prager yield criterion (see Jeong and Pan, 1995; Guo et al., 2008).

Most metallic alloys display plastic anisotropy as a result of forming processes. Recent studies have been devoted to the experimental characterization of the anisotropy of fracture in different alloys (see, for example, Benzerga et al., 2004a, for an overview of experimental evidence for anisotropic ductile fracture in steels). Liao et al. (1997) extended Gurson's (1977) cylindrical criterion to account for transverse isotropy by using Hill's (1948) yield criterion for the matrix material; however, these authors assumed that the anisotropy in the plane of the sheet is weak and can be described by a single anisotropy coefficient. Benzerga and Besson

(2001) extended Gurson's (1977) criterion for fully orthotropic metals. Upper-bound yield surfaces for both a hollow sphere and cylinder were deduced by assuming that the matrix material can be described using Hill's (1948) criterion with six non-zero anisotropy coefficients for three-dimensional stress conditions. Assuming triaxial loading conditions aligned with the material symmetry axes, closed-form approximate yield criteria were obtained for both spherical and cylindrical voids.

Numerical studies have been conducted to verify and validate these anisotropic Gurson-like criteria (e.g., Chien et al., 2001; Wang and Pan, 2004). Generally, finite-element analyses of a cube containing a spherical void, subjected to plane-stress conditions, were performed for various initial porosities and different values of the anisotropy parameters. More recently, these dilatational anisotropic plastic models have been used to predict forming limits for anisotropic sheets containing voids (see, for example, Brunet et al., 2004).

Note that the anisotropic models cited previously can describe the response of porous media only for particular void shapes (spherical or cylindrical) and axisymmetric loading conditions. It should be expected that void shape has a significant influence on the behavior of porous anisotropic metals, yet there have been relatively few studies on the combined effects of void shape and texture (see for example the experimental study of Benzerga et al. (2004a)). Benzerga et al. (2004b) proposed a yield criterion which combines properties from both Gologanu et al.'s (1993) criterion and Benzerga and Besson's (2001) criterion to account for both void shape (elliptical) and orthotropy, respectively. Recently, Monchiet et al. (2008) used a limit analysis approach to develop an analytical yield criterion for a matrix material obeying Hill's (1948) anisotropic yield criterion and containing elliptical voids. The limit analysis was performed for arbitrary deformation of the representative volume element. Furthermore, it was shown that for the case when the matrix is isotropic, Monchiet et al.'s (2008) criterion provides a rigorous generalization of the Gologanu et al. (1993) model. In Keralavarma and Benzerga (2010) further investigation into the evolution of the voids' orientation was provided.

All the studies cited so far assume that the yield strengths in tension and compression are equal in the void-free, or matrix, material. However, in the absence of voids, some materials with cubic crystal structure (see Benzerga et al., 2004a, for experimental data on high strength steels) are pressure-insensitive but exhibit tension–compression asymmetry in yielding. This shear related strength–differential (S–D) effect can result from single crystal plastic deformation due either to twinning or to slip that does not obey the well-known Schmid law (see, for example, Vitek et al., 2004; Hosford and Allen, 1973). Cazacu and Stewart (2009) recently extended Gurson's (1977) analysis to the case when the matrix material is incompressible but displays tension–compression asymmetry and developed an isotropic plastic potential for a porous aggregate that is sensitive to the third invariant of the stress deviator.

Metals with hexagonal crystal structure exhibit both tension–compression asymmetry and pronounced anisotropy. Experimental studies have shown that failure occurs by void growth and coalescence (see Huez et al., 1998). A fundamental issue that arises is how the texture and tension–compression asymmetry of the matrix influences the void growth stage of the failure process. A key ingredient in the development of a ductile failure model is an effective yield criterion. The aim of this paper is to develop a closed-form macroscopic yield criterion for anisotropic porous aggregates containing spherical voids using a micromechanical approach.

The structure of this article is as follows. In Section 2, the homogenization approach due to Hill (1967) and Mandel (1972) that is used in developing the macroscopic plastic potential for the void-matrix aggregate is presented. Next, the anisotropic Cazacu et al. (2006) yield criterion being used to model the rigid-plastic behavior of the matrix material in the void-matrix aggregate is recalled (see Section 3). Expressions for the macroscopic stresses and overall plastic dissipation are derived in Section 4. The main result of this paper, the expression of the analytical anisotropic plastic potential, is presented in Section 5. Finally, the accuracy of the developed criterion for plastic anisotropic media displaying strength–differential effects is assessed through comparison with numerical results obtained using finite element cell calculations (see Section 6).

2. Kinematic homogenization approach of Hill and Mandel

Consider a representative volume element Ω, composed of a homogeneous rigid-plastic matrix and a traction-free void. The matrix material is described by a convex yield function $\varphi(\boldsymbol{\sigma})$ in the stress space and an associated flow rule

$$\mathbf{d} = \dot{\lambda}\frac{\partial \varphi}{\partial \boldsymbol{\sigma}}, \tag{1}$$

where $\boldsymbol{\sigma}$ is the Cauchy stress tensor, $\dot{\lambda} \geqslant 0$ denotes the plastic multiplier rate and $\mathbf{d} = (1/2)(\nabla\mathbf{v} + \nabla\mathbf{v}^T)$ denotes the rate of deformation tensor with $\mathbf{v}$ being the velocity field. The yield surface is defined as $\varphi(\boldsymbol{\sigma}) = 0$. Let C denote the convex domain delimited by the yield surface such that

$$C = \{\boldsymbol{\sigma}|\varphi(\boldsymbol{\sigma}) \leqslant 0\}. \tag{2}$$

The plastic dissipation potential of the matrix is defined as

$$w(\mathbf{d}) = \sup_{\sigma \in C}(\boldsymbol{\sigma} : \mathbf{d}), \tag{3}$$

where ":" denotes the tensor double contraction. Uniform rate of deformation boundary conditions are assumed on the boundary of the RVE, $\partial\Omega$, such that

$$\mathbf{v} = \mathbf{D} \cdot \mathbf{x} \quad \text{for any} \quad \mathbf{x} \in \partial\Omega \tag{4}$$

with $\mathbf{D}$, the macroscopic rate of deformation tensor, being constant and $\mathbf{x}$ being the Cartesian position vector. For the boundary conditions given by Eq. (4), the Hill (1967), Mandel (1972) lemma applies; hence,

$$\langle \boldsymbol{\sigma} : \mathbf{d} \rangle_{\Omega} = \boldsymbol{\Sigma} : \mathbf{D}, \tag{5}$$

where $\langle \rangle$ denotes the average value over the representative volume Ω, and $\boldsymbol{\Sigma} = \langle \boldsymbol{\sigma} \rangle_{\Omega}$. Furthermore, there exists a macroscopic plastic dissipation potential $W(\mathbf{D})$ such that

$$\boldsymbol{\Sigma} = \frac{\partial W(\mathbf{D})}{\partial \mathbf{D}} \tag{6}$$

with

$$W(\mathbf{D}) = \inf_{\mathbf{d} \in K(\mathbf{D})} \langle w(\mathbf{d}) \rangle_{\Omega}, \tag{7}$$

where $K(\mathbf{D})$ is the set of incompressible velocity fields satisfying Eq. (4) (for more details see Gologanu et al., 1997; Leblond, 2003). This result will be further used to derive the plastic potential of the void-matrix aggregate in the case of a random distribution of spherical voids. To account simultaneously for anisotropy and tension–compression asymmetry associated with directional shear mechanisms at the single crystal level, the matrix material is assumed to obey the Cazacu et al. (2006) anisotropic yield criterion. This yield criterion and its dual in the strain rate space will be briefly presented next.

3. Anisotropic yield criterion for the matrix material

To account for both strength differential effects and anisotropy in pressure-insensitive hexagonal metals, Cazacu et al. (2006) proposed a 3-D orthotropic yield criterion (denoted in the following as CPB06). This criterion is an extension to orthotropy of the following isotropic yield function:

$$G(s_1, s_2, s_3; k, a) = (|s_1| - ks_1)^a + (|s_2| - ks_2)^a + (|s_3| - ks_3)^a \quad (8)$$

where s_1, s_2 and s_3 are the principal values of the stress deviator. The material parameter k captures strength differential effects while a is the degree of homogeneity. Starting from the isotropic function given by Eq. (8), anisotropy is then introduced through a linear transformation operating on the Cauchy stress deviator $\boldsymbol{\sigma}'$. The general form of the CPB06 anisotropic yield function is as follows:

$$F(\hat{\sigma}_1, \hat{\sigma}_2, \hat{\sigma}_3; k, a) = (|\hat{\sigma}_1| - k\hat{\sigma}_1)^a + (|\hat{\sigma}_2| - k\hat{\sigma}_2)^a + (|\hat{\sigma}_3| - k\hat{\sigma}_3)^a, \quad (9)$$

where $\hat{\sigma}_1, \hat{\sigma}_2$ and $\hat{\sigma}_3$ are the principal components of the transformed stress tensor

$$\hat{\boldsymbol{\sigma}} = \mathbf{L} : \boldsymbol{\sigma}'. \quad (10)$$

In Eq. (10), $\boldsymbol{\sigma}'$ is the Cauchy stress deviator and $\mathbf{L}$ is a fourth-order symmetric tensor invariant with respect to the orthotropy group. Thus, the yield condition can be written as

$$\sigma_e = \sigma_1^T, \quad (11)$$

where σ_e is the effective stress associated to the yield function of Eq. (9) and σ_1^T is the uniaxial tensile yield strength along an axis of orthotropy (e.g., the rolling direction). In other words,

$$\sigma_e = c_e \left[(|\hat{\sigma}_1| - k\hat{\sigma}_1)^a + (|\hat{\sigma}_2| - k\hat{\sigma}_2)^a + (|\hat{\sigma}_3| - k\hat{\sigma}_3)^a \right]^{1/a}, \quad (12)$$

where c_e is a constant defined such that σ_e reduces to the tensile yield stress along an axis of orthotropy.

In Cazacu et al. (2006), the physical significance of the coefficients involved in the CPB06 yield function given by Eq. (8) was presented and an identification procedure based on the results of tensile and compressive tests was outlined. It has been shown that the orthotropic CPB06 yield function given by Eq. (9) describes with accuracy the yield loci of various hexagonal materials (see, for example, Cazacu et al., 2006; Plunkett et al., 2008; Khan et al., 2007). For the magnesium alloys and zirconium materials, a value of the homogeneity parameter $a = 2$ (see Eq. (9)) approximates the plastic behavior best. Thus, in this paper $a = 2$ will be used in Eq. (9) to describe the yield behavior of the matrix. It is worth noting that if the material does not display tension–compression asymmetry, then the strength–differential parameter k is automatically equal to zero. If $k = 0$, $a = 2$ and $\mathbf{L}$ is constrained to be deviatoric, the CPB06 yield criterion reduces to that of Hill (1948).

3.1. Local stress potential

For $a = 2$, the effective stress of Eq. (12) becomes

$$\sigma_e = \hat{m} \sqrt{\sum_{i=1}^{3} (|\hat{\sigma}_i| - k\hat{\sigma}_i)^2}. \quad (13)$$

The constant $\hat{m}$ is defined such that σ_e reduces to the tensile yield stress along a specified axis of orthotropy. Due to the assumption of associated plastic flow, the stress potential for the matrix can be written as

$$\varphi(\hat{\boldsymbol{\sigma}}; \hat{m}, \sigma_1^T) = \hat{m} \sqrt{\sum_{i=1}^{3} (|\hat{\sigma}_i| - k\hat{\sigma}_i)^2} - \sigma_1^T = 0 \quad (14)$$

with material parameters σ_1^T and $\hat{m}$. As previously stated, the parameter σ_1^T is the uniaxial tensile yield strength along an axis of orthotropy while the constant $\hat{m}$ is defined such that Eq. (14) is identically satisfied for uniaxial tensile loading along this orthotropy axis.

Let $(\mathbf{e}_1, \mathbf{e}_2, \mathbf{e}_3)$ be the reference frame associated with orthotropy. In the case of a plate, $\mathbf{e}_1, \mathbf{e}_2$ and $\mathbf{e}_3$ represent the rolling, transverse and through-thickness directions, respectively. Relative to the orthotropy axes, the fourth-order tensor $\mathbf{L}$ (see Eq. (10)) is represented in Voigt notation by

$$\mathbf{L} = \begin{bmatrix} L_{11} & L_{12} & L_{13} & 0 & 0 & 0 \\ L_{12} & L_{22} & L_{23} & 0 & 0 & 0 \\ L_{13} & L_{23} & L_{33} & 0 & 0 & 0 \\ 0 & 0 & 0 & L_{44} & 0 & 0 \\ 0 & 0 & 0 & 0 & L_{55} & 0 \\ 0 & 0 & 0 & 0 & 0 & L_{66} \end{bmatrix}. \quad (15)$$

The constant $\hat{m}$ is expressible in terms of the anisotropy coefficients L_{ij} and the strength differential parameter k as

$$\hat{m} = \sqrt{\frac{1}{(|\Phi_1| - k\Phi_1)^2 + (|\Phi_2| - k\Phi_2)^2 + (|\Phi_3| - k\Phi_3)^2}}. \quad (16)$$

with

$$\begin{aligned} \Phi_1 &= \frac{2}{3}L_{11} - \frac{1}{3}L_{12} - \frac{1}{3}L_{13}, \\ \Phi_2 &= \frac{2}{3}L_{12} - \frac{1}{3}L_{22} - \frac{1}{3}L_{23}, \\ \Phi_3 &= \frac{2}{3}L_{13} - \frac{1}{3}L_{23} - \frac{1}{3}L_{33}. \end{aligned} \quad (17)$$

In the same spirit as Hill (1948), it is assumed here that the sum of the $\mathbf{L}$-components on the first row is equal to the sum of the $\mathbf{L}$-components on the second row and to the sum of the $\mathbf{L}$-components on the third row. Specifically,

$$\begin{aligned} L_{11} + L_{12} + L_{13} &= 1, \\ L_{12} + L_{22} + L_{23} &= 1, \\ L_{13} + L_{23} + L_{33} &= 1. \end{aligned} \quad (18)$$
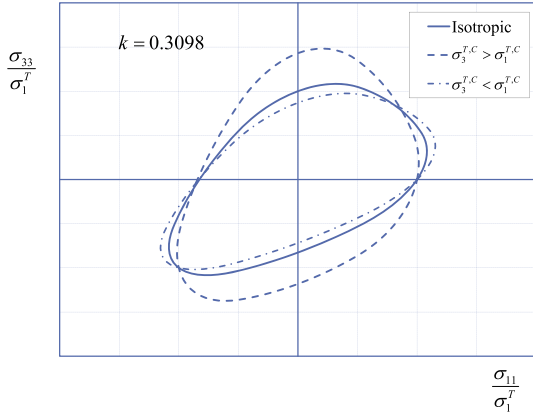
The constant on the right hand side of Eq. (18) has been chosen to be unity such that for isotropic conditions, the tensor $\mathbf{L}$ reduces to the fourth-order identity tensor, $\mathbf{1}$. Note that the additional constraints of Eq. (18) ensure that the transformed stress tensor $\hat{\boldsymbol{\sigma}}$ is deviatoric. As an example, in Fig. 1 is shown the representation in the biaxial plane $(\sigma_{11}, \sigma_{33})$ of the yield surface given by Eq. (14) corresponding to several materials displaying tension–compression asymmetry characterized by the same value of the strength–differential parameter $k = 0.3098$. One of these materials is isotropic while the other two materials are transversely isotropic with $(\mathbf{e}_1, \mathbf{e}_2)$ being the plane of symmetry (one material is stronger in the plane of symmetry while the other one is stronger in the direction normal to the symmetry plane, $\mathbf{e}_3$).

3.2. Local plastic dissipation

A key step in obtaining the overall plastic dissipation $W(\mathbf{D})$ of the void-matrix aggregate is the calculation of the local plastic dissipation $w(\mathbf{d})$ (see Eq. (3)) associated with the matrix yield criterion. Since the anisotropic criterion that describes yielding in the matrix is a homogeneous function of first order in stresses (see Eq. (14)), the local plastic dissipation becomes

$$w(\mathbf{d}) = \dot{\lambda}\sigma_1^T. \quad (19)$$

In other words, $\dot{\lambda}$ is the dual of the anisotropic stress potential φ given by Eq. (14).

Fig. 1. Plane stress yield loci for void-free materials according to the CPB06 yield criterion given by Eq. (14). The solid line denotes the isotropic material with the other curves represent the two transversely isotropic materials. All these materials display tension–compression asymmetry with $k = 0.3098$ (i.e., the tensile yield strengths are greater than the compressive yield strengths).

In the $(\mathbf{e}_1, \mathbf{e}_2, \mathbf{e}_3)$ frame associated with orthotropy, the transformed stress tensor of Eq. (10) can be written as

$$\hat{\sigma}_{mn} = L_{mnkl}\sigma'_{kl} = L_{mnkl}K_{klij}\sigma_{ij} \tag{20}$$

where $\mathbf{K}$ is the fourth-order deviatoric projection operator whose components with respect to any Cartesian coordinate system are

$$K_{ijkl} = \frac{1}{2}\left(\delta_{ik}\delta_{jl} + \delta_{il}\delta_{jk}\right) - \frac{\delta_{ij}\delta_{kl}}{3}. \tag{21}$$

In Voigt notation, $\mathbf{K}$ can be written as

$$\mathbf{K} = \frac{1}{3}\begin{bmatrix} 2 & -1 & -1 & 0 & 0 & 0 \\ -1 & 2 & -1 & 0 & 0 & 0 \\ -1 & -1 & 2 & 0 & 0 & 0 \\ 0 & 0 & 0 & 3 & 0 & 0 \\ 0 & 0 & 0 & 0 & 3 & 0 \\ 0 & 0 & 0 & 0 & 0 & 3 \end{bmatrix}. \tag{22}$$

Substituting the anisotropic stress potential given by Eq. (14) into the flow rule of Eq. (1) and applying the chain rule yields

$$d_{ij} = \dot{\lambda}\frac{\partial\varphi}{\partial\sigma_{ij}} = \dot{\lambda}\frac{\partial\varphi}{\partial\hat{\sigma}_{mn}}\frac{\partial\hat{\sigma}_{mn}}{\partial\sigma'_{rs}}\frac{\partial\sigma'_{rs}}{\partial\sigma_{ij}} = \dot{\lambda}\frac{\partial\varphi}{\partial\hat{\sigma}_{mn}}L_{mnrs}K_{rsij}. \tag{23}$$

Hence, in the anisotropic case,

$$B_{rsij}d_{ij} = \dot{\lambda}\frac{\partial\varphi}{\partial\hat{\sigma}_{rs}} \quad \text{when} \quad \varphi(\hat{\sigma}_1, \hat{\sigma}_2, \hat{\sigma}_3; \hat{m}, \sigma_1^T) = 0, \tag{24}$$

where the fourth-order tensor $\mathbf{B} = \mathbf{L}^{-1}$. Indeed, if the constraints given by Eq. (18) are enforced then $\mathbf{L}$ is invertible. Note that in the isotropic case,

$$d_{ij} = \dot{\lambda}_{iso}\frac{\partial\varphi}{\partial\sigma'_{ij}} \quad \text{when} \quad \varphi(s_1, s_2, s_3; m, \sigma_T) = 0, \tag{25}$$

where m is the isotropic version of $\hat{m}$ given by Eq. (16) and reduces to

$$m = \hat{m}|_{\mathbf{L=1}} = \sqrt{\frac{9/2}{3k^2 - 2k + 3}}. \tag{26}$$

The plastic multiplier rate associated with the isotropic CPB06 stress potential, $\dot{\lambda}_{iso}$, is expressed in terms of all principal values of the stress deviator (see Cazacu and Stewart, 2009). If $d_I \geqslant d_{II} \geqslant d_{III}$ are the principle values of the rate of deformation tensor $\mathbf{d}$, then the expression for the plastic multiplier rate is given as

$$\dot{\lambda}_{iso} = \begin{cases} \frac{1}{m(1+k)}\sqrt{\left(\frac{3k^2+10k+3}{3k^2-2k+3}\right)d_I^2 + d_{II}^2 + d_{III}^2} & \text{if } \frac{d_I}{\sqrt{d_{ij}d_{ij}}} \geqslant \frac{3k^2-2k+3}{\sqrt{6(k^2+3)(3k^2+1)}}, \\ \frac{1}{m(1-k)}\sqrt{d_I^2 + d_{II}^2 + \left(\frac{3k^2-10k+3}{3k^2+2k+3}\right)d_{III}^2} & \text{if } \frac{d_{III}}{\sqrt{d_{ij}d_{ij}}} \leqslant \frac{-(3k^2+2k+3)}{\sqrt{6(k^2+3)(3k^2+1)}}. \end{cases} \tag{27}$$

If $k = 0$ (no tension–compression asymmetry) then $\dot{\lambda}$ reduces to the von Mises effective strain rate ($\dot{\lambda} = \sqrt{(2/3)\mathbf{d}:\mathbf{d}}$). Comparing Eqs. (24) and (25), it follows that in the anisotropic case the expression for the plastic multiplier rate $\dot{\lambda}$ is obtained by replacing in Eq. (27) the rate of deformation tensor $\mathbf{d}$ with $\mathbf{b} = \mathbf{B}:\mathbf{d}$ and the constant m with $\hat{m}$. Thus, the anisotropic plastic multiplier rate is given as follows:

$$\dot{\lambda} = \begin{cases} \frac{1}{\hat{m}(1+k)}\sqrt{\left(\frac{3k^2+10k+3}{3k^2-2k+3}\right)b_I^2 + b_{II}^2 + b_{III}^2} & \text{if } \frac{b_I}{\sqrt{b_{ij}b_{ij}}} \geqslant \frac{3k^2-2k+3}{\sqrt{6(k^2+3)(3k^2+1)}}, \\ \frac{1}{\hat{m}(1-k)}\sqrt{b_I^2 + b_{II}^2 + \left(\frac{3k^2-10k+3}{3k^2+2k+3}\right)b_{III}^2} & \text{if } \frac{b_{III}}{\sqrt{b_{ij}b_{ij}}} \leqslant \frac{-(3k^2+2k+3)}{\sqrt{6(k^2+3)(3k^2+1)}}, \end{cases} \tag{28}$$

where b_I, b_{II} and b_{III} are the ordered principal components of b_{ij} (for more details see Cazacu et al., 2010). It is worth noting that if there is no tension–compression asymmetry in the matrix material (i.e., the yield strength in tension is equal to the yield in compression) then the parameter k associated with strength differential effects is automatically zero. Therefore, the anisotropic strain rate potential given by Eq. (28) reduces to $\dot{\lambda} = \sqrt{\mathbf{b}:\mathbf{b}}/\hat{m}$, which can be rewritten as $\dot{\lambda} = \sqrt{(2/3)\mathbf{d}:\mathbf{H}:\mathbf{d}}$ with $\mathbf{H}$ being a fourth-order orthotropic tensor satisfying $H_{iikl} = 0$ with $i = 1, 2, 3$. Thus, if $k = 0$, Eq. (28) reduces to Hill's (1987) orthotropic strain rate potential.

Note that the scalar $\mathbf{b}:\mathbf{b}$, which appears in Eq. (28), can be expressed as follows:

$$\mathbf{b} : \mathbf{b} = \mathbf{d} : \widehat{\mathbf{L}} : \mathbf{d} \tag{29}$$

where $\widehat{\mathbf{L}}$ is a fourth-order diagonal tensor in the coordinate system associated to the material symmetry $(\mathbf{e}_1, \mathbf{e}_2, \mathbf{e}_3)$ and is expressible in Voigt notation as

$$\widehat{\mathbf{L}} = \begin{bmatrix} \hat{l}_1 & 0 & 0 & 0 & 0 & 0 \\ 0 & \hat{l}_2 & 0 & 0 & 0 & 0 \\ 0 & 0 & \hat{l}_3 & 0 & 0 & 0 \\ 0 & 0 & 0 & \hat{l}_4 & 0 & 0 \\ 0 & 0 & 0 & 0 & \hat{l}_5 & 0 \\ 0 & 0 & 0 & 0 & 0 & \hat{l}_6 \end{bmatrix}. \tag{30}$$

The expressions for the diagonal components of $\widehat{\mathbf{L}}$ in terms of the components of $\mathbf{B} = \mathbf{L}^{-1}$ are

$$\hat{l}_1 = B_{11}^2 + B_{12}^2 + B_{13}^2 - B_{11}B_{12} - B_{11}B_{13} - B_{22}B_{12} + B_{22}B_{23} - B_{33}B_{13}$$
$$+ B_{33}B_{23} + B_{12}B_{13} - B_{12}B_{23} - B_{13}B_{23}$$

$$\hat{l}_2 = B_{12}^2 + B_{22}^2 + B_{23}^2 - B_{22}B_{12} - B_{22}B_{23} - B_{11}B_{12} + B_{11}B_{13} - B_{33}B_{23}$$
$$+ B_{33}B_{13} + B_{12}B_{23} - B_{23}B_{13} - B_{12}B_{13}$$

$$\hat{l}_3 = B_{13}^2 + B_{23}^2 + B_{33}^2 - B_{33}B_{13} - B_{33}B_{23} - B_{11}B_{13} + B_{11}B_{12} - B_{22}B_{23}$$
$$+ B_{22}B_{12} + B_{13}B_{23} - B_{12}B_{13} - B_{23}B_{12}$$

$$\hat{l}_4 = B_{44}^2$$

$$\hat{l}_5 = B_{55}^2$$

$$\hat{l}_6 = B_{66}^2. \tag{31}$$

4. Development of the anisotropic macroscopic yield criterion

An approximate yield criterion will now be analytically derived for a void-matrix aggregate containing randomly-distributed

spherical voids and with an incompressible matrix material displaying anisotropy and tension–compression asymmetry. The matrix yield behavior will be described using the criterion given by Eq. (14). The approach that will be used in the derivation is the kinematic homogenization approach presented in Section 2.

Consider as an RVE a hollow sphere with inner radius a and outer radius $b = af^{-1/3}$, where f is the void volume fraction (also called the porosity). The void is considered to be traction-free. The RVE is subjected to axisymmetric loading such that

$$\Sigma = \Sigma_{11}(\mathbf{e}_1 \otimes \mathbf{e}_1 + \mathbf{e}_2 \otimes \mathbf{e}_2) + \Sigma_{33}(\mathbf{e}_3 \otimes \mathbf{e}_3), \tag{32}$$

where $\Sigma = \langle \boldsymbol{\sigma} \rangle_\Omega$ denotes the macroscopic stress tensor while $(\mathbf{e}_1, \mathbf{e}_2, \mathbf{e}_3)$ is the frame associated to the axes of orthotropy.

To obtain the upper-bound of the overall plastic potential, the classical velocity field proposed by Rice and Tracey (1969) and Gurson (1977) will be used. Thus, the local velocity field $\mathbf{v}$ in the RVE is considered to be of the form

$$\mathbf{v} = \mathbf{v}^V + \mathbf{v}^S, \tag{33}$$

where $\mathbf{v}^V$ is associated with volumetric expansion and $\mathbf{v}^S$ is associated with shape changes. Imposing uniform rate of deformation boundary conditions and matrix incompressibility yields

$$\mathbf{v}(\mathbf{x} = b\mathbf{e}_r) = \mathbf{D} \cdot \mathbf{x} \quad \text{and} \quad \text{div}\,\mathbf{v} = 0, \tag{34}$$

where $\mathbf{x}$ is the Cartesian position vector that denotes the current position in the RVE and $\mathbf{e}_r$ is the radial unit vector.

From Eqs. (33) and (34), it follows that

$$\mathbf{v}^V = D_m \left(\frac{b^3}{r^2}\right) \mathbf{e}_r,$$

$$\mathbf{v}^S = \mathbf{D}' \cdot \mathbf{x}, \tag{35}$$

where r is the radial coordinate, $D_m = \frac{1}{3} D_{kk}$ is the mean part of $\mathbf{D}$ and $\mathbf{D}' = \mathbf{D} - D_m\mathbf{I}$ is the deviatoric part of $\mathbf{D}$ with $\mathbf{I}$ being the second-order identity tensor. In Eq. (35), both Cartesian and spherical coordinates have been used. The local rate of deformation tensor $\mathbf{d} = \frac{1}{2}(\nabla\mathbf{v} + \nabla^T\mathbf{v})$ corresponding to the velocity field $\mathbf{v}$ given by Eq. (35) is

$$\mathbf{d} = \mathbf{d}^V + \mathbf{d}^S, \tag{36}$$

where

$$\mathbf{d}^S = \mathbf{D}',$$

$$\mathbf{d}^V = D_m \left(\frac{b}{r}\right)^3 \left(-2\mathbf{e}_r \otimes \mathbf{e}_r + \mathbf{e}_\theta \otimes \mathbf{e}_\theta + \mathbf{e}_\phi \otimes \mathbf{e}_\phi\right)$$

$$= D_m \left(\frac{b}{r}\right)^3 \bar{\mathbf{d}}, \tag{37}$$

with $\bar{\mathbf{d}} = (-2\mathbf{e}_r \otimes \mathbf{e}_r + \mathbf{e}_\theta \otimes \mathbf{e}_\theta + \mathbf{e}_\phi \otimes \mathbf{e}_\phi)$. Hence, the principal values of the local rate of deformation tensor $\mathbf{d}$ are as follows:

$$d_1 = D_m \left(\frac{b}{r}\right)^3 + D'_{11},$$

$$d_2 = -\frac{1}{2}\left[D_m \left(\frac{b}{r}\right)^3 + D'_{11}\right]$$
$$+ \frac{3}{2}\sqrt{D_m^2 \left(\frac{b}{r}\right)^6 + 2D'_{11}D_m \left(\frac{b}{r}\right)^3 \cos 2\theta + (D'_{11})^2}, \tag{38}$$

$$d_3 = -\frac{1}{2}\left[D_m \left(\frac{b}{r}\right)^3 + D'_{11}\right]$$
$$- \frac{3}{2}\sqrt{D_m^2 \left(\frac{b}{r}\right)^6 + 2D'_{11}D_m \left(\frac{b}{r}\right)^3 \cos 2\theta + (D'_{11})^2}.$$

4.1. Overall plastic dissipation

Let $W^+(\mathbf{D})$ denote the average macroscopic plastic dissipation corresponding to the velocity field given by Eq. (35) such that

$$W^+(\mathbf{D}) = \frac{1}{V}\int_{\Omega-\omega} w(\mathbf{d})dV = \frac{1}{V}\int_{\Omega-\omega} \sigma_1^T \dot{\lambda}\,dV, \tag{39}$$

where $\mathbf{d}$ is given by Eqs. (36) and (37), $V = \frac{4}{3}\pi b^3$ is the volume of the RVE being considered, ω represents the void volume and $\dot{\lambda}$ is the plastic multiplier rate associated to the anisotropic CPB06 yield criterion (see Eq. (28)). The approach of Leblond (2003) will be followed to obtain a new upper-bound estimate of the macroscopic yield locus by applying the Cauchy–Schwartz inequality as follows:

$$W^+(\mathbf{D}) = \frac{1}{V}\int_a^b 4\pi r^2 \langle w(\mathbf{d})\rangle_{S(r)}dr$$
$$\leqslant W^{++}(\mathbf{D}) = \frac{1}{V}\int_a^b 4\pi r^2 \left[\langle w^2(\mathbf{d})\rangle_{S(r)}\right]^{1/2}dr, \tag{40}$$

where $S(r)$ is the spherical surface of radius r. In Eq. (40), the following notation was used for averaging over $S(r)$:

$$\langle x \rangle_{S(r)} = \frac{1}{4\pi}\int_0^{2\pi}\int_0^\pi x \sin\theta d\theta d\phi. \tag{41}$$

When the matrix behavior is described by the von Mises yield criterion ($\mathbf{L} = \mathbf{1}$, $k = 0$), $W^{++}(\mathbf{D})$ can be evaluated analytically (see Gurson, 1977; Leblond, 2003). In the current derivation, fresh difficulties are encountered when estimating the overall local plastic dissipation $w(\mathbf{d})$. These difficulties are due to the tension–compression asymmetry and anisotropy of the matrix material and are associated with the fact that the CPB06 plastic multiplier rate has multiple branches (see Eq. (28)). The expression for the CPB06 plastic multiplier rate depends on the sign and ordering of the principal values of the transformed rate of deformation tensor $\mathbf{b} = \mathbf{B}{:}\mathbf{d}$.

For the case of an isotropic matrix exhibiting tension–compression asymmetry ($\mathbf{L} = \mathbf{1}$ but $k \neq 0$), the expressions for the local plastic dissipation are provided in Cazacu and Stewart (2009). In order to obtain an analytic expression of the integral representing the overall plastic dissipation, it was assumed that in the expressions of the local plastic dissipation (see, for example, Eqs. (24)–(30) of Cazacu and Stewart, 2009), the cross term $D_mD'_{11}$ could be neglected. Note that the upper-bound character of the criterion is retained for both the purely deviatoric or purely hydrostatic cases (since the cross term is zero for both loading conditions). The validity of the approximation for general loadings was assessed in Cazacu and Stewart (2009) by conducting finite-element cell calculations. Using this approximation, the isotropic local plastic dissipation becomes (see Eqs. (19), (27) and (38)):

$$w(\mathbf{d}) = \sigma_1^T \sqrt{n d_{ij} d_{ij}}, \tag{42}$$

where

$$n = \begin{cases} \frac{1}{m^2}\left(\frac{3}{3k^2 - 2k + 3}\right) & \text{if } \Sigma_m < 0, \\ \frac{1}{m^2}\left(\frac{3}{3k^2 + 2k + 3}\right) & \text{if } \Sigma_m > 0, \end{cases} \tag{43}$$

and Σ_m is the applied mean stress. Note that for the cases of purely hydrostatic and purely deviatoric loading, the approximation given by Eq. (42) coincides with the exact value of the local plastic dissipation for the velocity field given by Eq. (35).

In the anisotropic case, the local plastic dissipation is obtained by replacing in Eq. (42) the local rate of deformation tensor $\mathbf{d}$ with the transformed rate of deformation tensor $\mathbf{b} = \mathbf{B}{:}\mathbf{d}$ and the constant n with its anisotropic equivalent $\hat{n}$. Thus, the following

approximate form of the plastic multiplier rate will be used when calculating the overall plastic dissipation W++ (see Eq. (40)):

$$\dot{\lambda}^2 = \hat{n} b_{ij} b_{ij} \tag{44}$$

such that

$$w(\mathbf{d}) = \sigma_1^T \sqrt{\hat{n} b_{ij} b_{ij}}, \tag{45}$$

where

$$\hat{n} = \begin{cases} \frac{1}{\hat{m}^2}\left(\frac{3}{3k^2 - 2k + 3}\right) & \text{if } \Sigma_m < 0, \\ \frac{1}{\hat{m}^2}\left(\frac{3}{3k^2 + 2k + 3}\right) & \text{if } \Sigma_m > 0. \end{cases} \tag{46}$$

4.2. Macroscopic stresses

Let $\tilde{\Sigma}_e$ denote the macroscopic effective stress associated to the CPB06 anisotropic potential as

$$\tilde{\Sigma}_e = \hat{m}\sqrt{\sum_{i=1}^{3}\left(|\hat{\Sigma}_i| - k\hat{\Sigma}_i\right)^2} \tag{47}$$

where $\hat{\Sigma} = \mathbf{L} : \Sigma'$ is the transformed macroscopic stress tensor. The effective strain rate associated with the CPB06 stress potential will be denoted by $\tilde{D}_e$. A rigorous proof that $\tilde{D}_e$ is a work-conjugate measure of $\tilde{\Sigma}_e$ (i.e., that $\tilde{\Sigma}_e \tilde{D}_e = \Sigma' : \mathbf{D}'$) was provided in Cazacu et al. (2010). According to Eqs. (29) and (44)

$$\tilde{D}_e = \dot{\lambda}(\mathbf{D}') = \sqrt{\hat{n}\left(\mathbf{D}' : \widehat{\mathbf{L}} : \mathbf{D}'\right)}. \tag{48}$$

Let $\Sigma_e = \sqrt{(3/2)\Sigma'_{ij}\Sigma'_{ij}}$ and $D_e = \sqrt{(2/3)D'_{ij}D'_{ij}}$ denote the von Mises effective stress and the von Mises effective strain rate, respectively. For an orthotropic material under axisymmetric loading conditions (see Eq. (35)), the von Mises effective stress is related to the CPB06 effective stress as

$$\Sigma_e = g\tilde{\Sigma}_e \tag{49}$$

where g is a constant (see Eq. (75)) expressible in terms of the strength differential parameter k and the components of the anisotropic tensor $\mathbf{L}$. Since $\tilde{D}_e$ is a work-conjugate measure of $\tilde{\Sigma}_e$ and Σ_e is a work-conjugate measure of D_e, it follows that

$$D_e = \frac{1}{g}\tilde{D}_e. \tag{50}$$

The macroscopic stress tensor associated with the upper-bound estimate of the plastic dissipation $W^{++}(\mathbf{D})$ is given as

$$\mathbf{\Sigma} = \frac{\partial W^{++}}{\partial \mathbf{D}}(D_m, D_e). \tag{51}$$

Employing the chain rule yields

$$\mathbf{\Sigma} = \frac{\partial W^{++}}{\partial D_m}\frac{\partial D_m}{\partial \mathbf{D}} + \frac{\partial W^{++}}{\partial D_e}\frac{\partial D_e}{\partial \mathbf{D}} \tag{52}$$

such that

$$\Sigma_m = \frac{1}{3}\frac{\partial W^{++}}{\partial D_m} \tag{53}$$

and

$$\mathbf{\Sigma}' = \frac{2}{3}\frac{\mathbf{D}'}{D_e}\frac{\partial W^{++}}{\partial D_e}. \tag{54}$$

It follows that

$$\Sigma_e = \left|\frac{\partial W^{++}}{\partial D_e}\right| \tag{55}$$

and

$$\frac{\partial W^{++}}{\partial \tilde{D}_e} = \frac{1}{g}\frac{\partial W^{++}}{\partial D_e} \tag{56}$$

such that

$$\tilde{\Sigma}_e = \left|\frac{\partial W^{++}}{\partial \tilde{D}_e}\right|. \tag{57}$$

5. Anisotropic criterion

According to Eq. (37), the local rate of deformation can be decomposed into a volumetric part $\mathbf{d}^V$ and a deviatoric part $\mathbf{d}^S = \mathbf{D}' = $ constant. Thus, the approximate expression for the macroscopic plastic dissipation can be written as

$$\begin{aligned} W^{++} &= \frac{\sigma_1^T}{V}\int_a^b 4\pi r^2 \left[\langle\dot{\lambda}^2\rangle_{S(r)}\right]^{1/2} dr \\ &= \frac{\sigma_1^T}{V}\int_a^b 4\pi r^2 \left[\hat{n}\langle\mathbf{b} : \mathbf{b}\rangle_{S(r)}\right]^{1/2} dr \\ &= \frac{\sigma_1^T}{V}\int_a^b 4\pi r^2 \left[\hat{n}\langle\mathbf{d} : \widehat{\mathbf{L}} : \mathbf{d}\rangle_{S(r)}\right]^{1/2} dr \\ &= \frac{\sigma_1^T}{V}\int_a^b 4\pi r^2 \left[\hat{n}\langle\mathbf{d}^V : \widehat{\mathbf{L}} : \mathbf{d}^V + \mathbf{d}^S : \widehat{\mathbf{L}} : \mathbf{d}^S + 2\mathbf{d}^V : \widehat{\mathbf{L}} : \mathbf{d}^S\rangle_{S(r)}\right]^{1/2} dr. \end{aligned} \tag{58}$$

Since

$$\langle\mathbf{d}^S : \widehat{\mathbf{L}} : \mathbf{d}^S\rangle_{S(r)} = \mathbf{D}' : \widehat{\mathbf{L}} : \mathbf{D}' \tag{59}$$

and noting that

$$\langle\mathbf{d}^V : \widehat{\mathbf{L}} : \mathbf{d}^S\rangle_{S(r)} = \langle\mathbf{d}^V\rangle_{S(r)} : \widehat{\mathbf{L}} : \mathbf{D}' \tag{60}$$

with

$$\langle\bar{\mathbf{d}}\rangle_{S(r)} = \langle[-2\mathbf{e}_r \otimes \mathbf{e}_r + \mathbf{e}_\theta \otimes \mathbf{e}_\theta + \mathbf{e}_\phi \otimes \mathbf{e}_\phi]\rangle_{S(r)} = \mathbf{0}, \tag{61}$$

the following expression is obtained for the estimated macroscopic plastic dissipation:

$$\begin{aligned} W^{++} &= \frac{\sigma_1^T}{\frac{4}{3}\pi b^3}\int_a^b 4\pi r^2 \left[\hat{n}\langle\mathbf{d}^V : \widehat{\mathbf{L}} : \mathbf{d}^V\rangle_{S(r)} + \hat{n}\mathbf{D}' : \widehat{\mathbf{L}} : \mathbf{D}'\right]^{1/2} dr \\ &= \frac{3\sigma_1^T}{b^3}\int_a^b r^2 \sqrt{D_m^2\frac{b^6}{r^6}h^2 + \tilde{D}_e^2}\, dr \\ &= \sigma_1^T |D_m| h\int_1^{1/f} \sqrt{u^2 + \frac{1}{\gamma^2}\frac{1}{u^2}}\, du \end{aligned} \tag{62}$$

such that

$$W^{++} = \sigma_1^T |D_m| h\left[\sinh^{-1}(\gamma u) - \frac{\sqrt{1 + \gamma^2 u^2}}{\gamma u}\right]_1^{1/f}, \tag{63}$$

where $u = b^3/r^3$,

$$\gamma = \frac{|D_m|}{\tilde{D}_e}h \tag{64}$$

and

$$h^2 = \hat{n}\langle\bar{\mathbf{d}} : \widehat{\mathbf{L}} : \bar{\mathbf{d}}\rangle_{S(r)} = \hat{n}\left[\frac{4}{5}\left(\hat{l}_1 + \hat{l}_2 + \hat{l}_3\right) + \frac{6}{5}\left(\hat{l}_4 + \hat{l}_5 + \hat{l}_6\right)\right] \tag{65}$$

(see Appendix A for details regarding the calculation of h). Note that the parameter h depends on the anisotropy coefficients (see Eq. (15)) as well as the parameter $\hat{n}$ given by Eq. (46).

Using Eqs. (53) and (57) along with Eq. (63) yields

$$
\begin{aligned}
\Sigma_m &= \frac{1}{3}\frac{\partial W^{++}}{\partial D_m} = \frac{h}{3}\sigma_1^T \mathrm{sgn}(D_m)\left[\sinh^{-1}(\gamma u)\right]_1^{1/f} \\
&= \frac{h}{3}\sigma_1^T \mathrm{sgn}(D_m)\left[\sinh^{-1}\left(\frac{\gamma}{f}\right) - \sinh^{-1}(\gamma)\right]
\end{aligned}
\tag{66}
$$

and

$$
\tilde{\Sigma}_e = \left|\frac{\partial W^{++}}{\partial \tilde{D}_e}\right| = \sigma_1^T\left|\frac{\sqrt{1+\gamma^2 u^2}}{u}\right|_1^{1/f} = \sigma_1^T\left|\sqrt{1+\gamma^2} - \sqrt{\gamma^2+f^2}\right|.
\tag{67}
$$

Finally, eliminating γ from the previous two equations yields the following expression for the macroscopic yield criterion incorporating anisotropy:

$$
\Phi = \left(\frac{\hat{m}\sqrt{\sum_{i=1}^{3}\left(|\hat{\Sigma}_i| - k\hat{\Sigma}_i\right)^2}}{\sigma_1^T}\right)^2 + 2f\cosh\left(\frac{3\Sigma_m}{h\sigma_1^T}\right) - 1 - f^2 = 0,
\tag{68}
$$

where $\hat{\boldsymbol{\Sigma}} = \mathbf{L}:\boldsymbol{\Sigma}$, σ_1^T is the uniaxial tensile yield strength in the 1-direction of orthotropy, f is the void volume fraction, Σ_m is the macroscopic mean stress, h is the hydrostatic factor given by Eq. (65) and the parameter $\hat{m}$ is given by Eq. (16). These key equations are repeated here for the readers convenience:

$$
\hat{m} = \sqrt{\frac{1}{(|\Phi_1| - k\Phi_1)^2 + (|\Phi_2| - k\Phi_2)^2 + (|\Phi_3| - k\Phi_3)^2}}
\tag{16}
$$

with

$$
\begin{aligned}
\Phi_1 &= \frac{2}{3}L_{11} - \frac{1}{3}L_{12} - \frac{1}{3}L_{13}, \\
\Phi_2 &= \frac{2}{3}L_{12} - \frac{1}{3}L_{22} - \frac{1}{3}L_{23}, \\
\Phi_3 &= \frac{2}{3}L_{13} - \frac{1}{3}L_{23} - \frac{1}{3}L_{33}
\end{aligned}
\tag{17}
$$

and

$$
h^2 = \hat{n}\langle\bar{\mathbf{d}}:\widehat{\mathbf{L}}:\bar{\mathbf{d}}\rangle_{S(r)} = \hat{n}\left[\frac{4}{5}\left(\hat{l}_1 + \hat{l}_2 + \hat{l}_3\right) + \frac{6}{5}\left(\hat{l}_4 + \hat{l}_5 + \hat{l}_6\right)\right]
\tag{65}
$$

with

$$
\begin{aligned}
\hat{l}_1 &= B_{11}^2 + B_{12}^2 + B_{13}^2 - B_{11}B_{12} - B_{11}B_{13} - B_{22}B_{12} + B_{22}B_{23} - B_{33}B_{13} \\
&\quad + B_{33}B_{23} + B_{12}B_{13} - B_{12}B_{23} - B_{13}B_{23} \\
\hat{l}_2 &= B_{12}^2 + B_{22}^2 + B_{23}^2 - B_{22}B_{12} - B_{22}B_{23} - B_{11}B_{12} + B_{11}B_{13} - B_{33}B_{23} \\
&\quad + B_{33}B_{13} + B_{12}B_{23} - B_{23}B_{13} - B_{12}B_{13} \\
\hat{l}_3 &= B_{13}^2 + B_{23}^2 + B_{33}^2 - B_{33}B_{13} - B_{33}B_{23} - B_{11}B_{13} + B_{11}B_{12} - B_{22}B_{23} \\
&\quad + B_{22}B_{12} + B_{13}B_{23} - B_{12}B_{13} - B_{23}B_{12} \\
\hat{l}_4 &= B_{44}^2 \\
\hat{l}_5 &= B_{55}^2 \\
\hat{l}_6 &= B_{66}^2,
\end{aligned}
\tag{31}
$$

where $\mathbf{B} = \mathbf{L}^{-1}$.

Note that the developed criterion (Eq. (68)) accounts for the combined effects of matrix anisotropy and tension–compression asymmetry on both the yielding of the porous aggregate and the porosity evolution. These effects are captured through the strength–differential parameter k and the anisotropy coefficients (the components of the fourth-order tensor $\mathbf{L}$) involved in the expressions of the transformed stress tensor $\hat{\sigma}$ as well as $\hat{m}$ and h. Indeed, the evolution of the porosity is given as

$$
\begin{aligned}
\dot{f} &= (1-f)D_{kk}^P = (1-f)\dot{\lambda}\frac{\partial\Phi}{\partial\Sigma_{kk}} \\
&= (1-f)\dot{\lambda}\left(\frac{6f}{h\sigma_1^T}\right)\sinh\left(\frac{3\Sigma_m}{h\sigma_1^T}\right).
\end{aligned}
\tag{69}
$$

Eq. (68) represents the approximate yield criterion for a porous material with the matrix incompressible, orthotropic and displaying tension–compression asymmetry. Although the expression of the developed criterion is similar to that of Benzerga and Besson (2001), there are distinct differences. First, Hill's (1948) effective stress is replaced with the CPB06 effective stress $\tilde{\Sigma}_e$, which involves the stress deviator $\boldsymbol{\Sigma}'$, the anisotropy coefficients L_{ij} and the strength–differential parameter k. Secondly, the hydrostatic parameter h depends on the anisotropy coefficients L_{ij}, on the strength–differential parameter k and on the sign of the applied mean stress Σ_m.

In contrast with the criteria of Gurson (1977) and that of Benzerga and Besson (2001), the yield locus given by Eq. (68) is no longer symmetric with respect to the axis $\Sigma_m = 0$. According to the developed criterion, for tensile hydrostatic loading, yielding occurs in the porous aggregate when $\Sigma_m = p_Y^+$ with

$$
p_Y^+ = -\sigma_1^T\sqrt{\frac{2}{15\hat{m}^2}\left(\frac{7\hat{l}_1 + 2\hat{l}_3 + 6\hat{l}_4}{3k^2 + 2k + 3}\right)}\ln(f),
\tag{70}
$$

while for compressive loading yielding occurs when $\Sigma_m = p_Y^-$ with

$$
p_Y^- = \sigma_1^T\sqrt{\frac{2}{15\hat{m}^2}\left(\frac{7\hat{l}_1 + 2\hat{l}_3 + 6\hat{l}_4}{3k^2 - 2k + 3}\right)}\ln(f).
\tag{71}
$$

If there is no tension–compression asymmetry in the matrix ($k = 0$), $p_Y^+ = |p_y^-|$. The limiting pressures p_y^+ and p_y^- correspond to the exact solution of a hollow sphere loaded hydrostatically only if the matrix is isotropic ($\mathbf{L} = \mathbf{1}$) since, in this case, the trial velocity field given by Eq. (35) is the only admissible velocity field.

If the matrix is orthotropic and has no tension–compression asymmetry, Eq. (68) reduces to that of Benzerga and Besson (2001). Indeed, for $k = 0$, $\hat{n} = 2/3$ and $\widehat{\mathbf{L}} = \widehat{\mathbf{H}}$ (i.e., the matrix behavior is described by Hill's 1948 yield criterion), the hydrostatic factor h given by Eq. (65) reduces to

$$
h = \sqrt{\frac{8}{15}\left(\hat{l}_1 + \hat{l}_2 + \hat{l}_3\right) + \frac{4}{5}\left(\hat{l}_4 + \hat{l}_5 + \hat{l}_6\right)},
\tag{72}
$$

which is the hydrostatic factor corresponding to a Hill (1948) matrix (see Benzerga and Besson, 2001). Note that when the matrix is isotropic and displays tension–compression asymmetry (i.e., $\widehat{\mathbf{L}} = \mathbf{I}$ and $k \neq 0$),

$$
h = \begin{cases} 2 & \text{if } \Sigma_m < 0, \\ 2\sqrt{\frac{3k^2 - 2k + 3}{3k^2 + 2k + 3}} & \text{if } \Sigma_m > 0 \end{cases}
\tag{73}
$$

such that the developed criterion (Eq. (68)) reduces to that proposed in Cazacu and Stewart (2009). Furthermore, for a von Mises matrix ($\widehat{\mathbf{L}} = \mathbf{I}$ and $k = 0$) the developed criterion reduces to Gurson's (1977) yield criterion for spherical voids. In the next section, the capabilities of the developed model will be further illustrated and comparisons with finite element calculations will be made to validate the predicted yield behavior.

6. Validation of the developed anisotropic criterion

This section focuses on the assessment of the developed anisotropic criterion given by Eq. (68). The model is analyzed in detail for some specific materials in Section 6.1, axisymmetric unit cell finite element (FE) calculations are presented in Section 6.2 and

comparisons between the finite element results and the materials analyzed previously are given in Section 6.3.

6.1. Model assessment

The following analysis will focus on the case of transversely isotropic materials. The choice of a simplified material orthotropy representation (i.e., the plane of symmetry e_1e_2 is isotropic) is considered because the discussion for general orthotropy would involve a very high number of materials corresponding to different values for the anisotropy coefficients L_{ij} (i.e. various orderings of the tensile and compressive yield stresses corresponding to the directions e_1, e_2, e_3). Transverse isotropy is common in clock-rolled hexagonal metal sheets, where multiple passes ensure in-plane isotropy (see, for example, the data on high-purity zirconium reported in Tomé et al., 2001; Nixon, 2008). For a given loading path, the parameters that are varied are the anisotropy coefficients L_{ij} and the tension–compression parameter k. Thus, the yield surfaces of nine materials containing randomly oriented spherical voids will be examined:

1. Isotropic materials for which the matrix is characterized by **L = 1** and either displays tension–compression asymmetry (such that $k \neq 0$) or does not ($k = 0$). These materials are called materials type A.
2. Transversely isotropic materials for which the matrix has a weaker in-plane yield strength than through-thickness yield strength (see Fig. 2) with either tension–compression asymmetry ($k \neq 0$) or not ($k = 0$). These materials are called materials type B.

3. Transversely isotropic materials with matrix displaying larger in-plane yield strength than through-thickness yield strength (see Fig. 2) with either tension–compression asymmetry ($k \neq 0$) or not ($k = 0$). These materials are called materials type C.

The isotropic case (material type A) is taken as a reference. Note that calculations for material A with $k = 0$ corresponds to a von Mises matrix; hence, the FE results obtained in this case will be compared to the Gurson–Tvergaard–Needleman (GTN) yield locus. Likewise, material type A with $k \neq 0$ corresponds to the isotropic CPB06 matrix and FE results will be compared to the Cazacu and Stewart (2009) yield locus. In Table 1 are given the numerical values of the anisotropy coefficients for each material. These values were chosen such that all materials have the same tensile yield strength in the plane of symmetry. As an example, in Fig. 2 are represented the projection of the yield loci given by Eq. (68) corresponding to $f = 0$ (the void-free state) for all these materials.

As already mentioned, if the anisotropic matrix does not display tension–compression asymmetry ($k = 0$), then the developed criterion of Eq. (68) reduces to that proposed by Benzerga and Besson (2001) for spherical void geometry. In Benzerga and Besson (2001), through comparison with axisymmetric cell calculations, the authors have assessed the accuracy of the description of the effects of plastic anisotropy on void growth. However, no discussion of the accuracy of the yielding description has been reported.

In this paper, the numerical values for the anisotropy coefficients of the transversely isotropic materials B and C with no tension–compression asymmetry were taken to coincide with the set of anisotropy parameters considered by Benzerga and Besson (2001), which correspond to a zircaloy sheet and thin aluminum
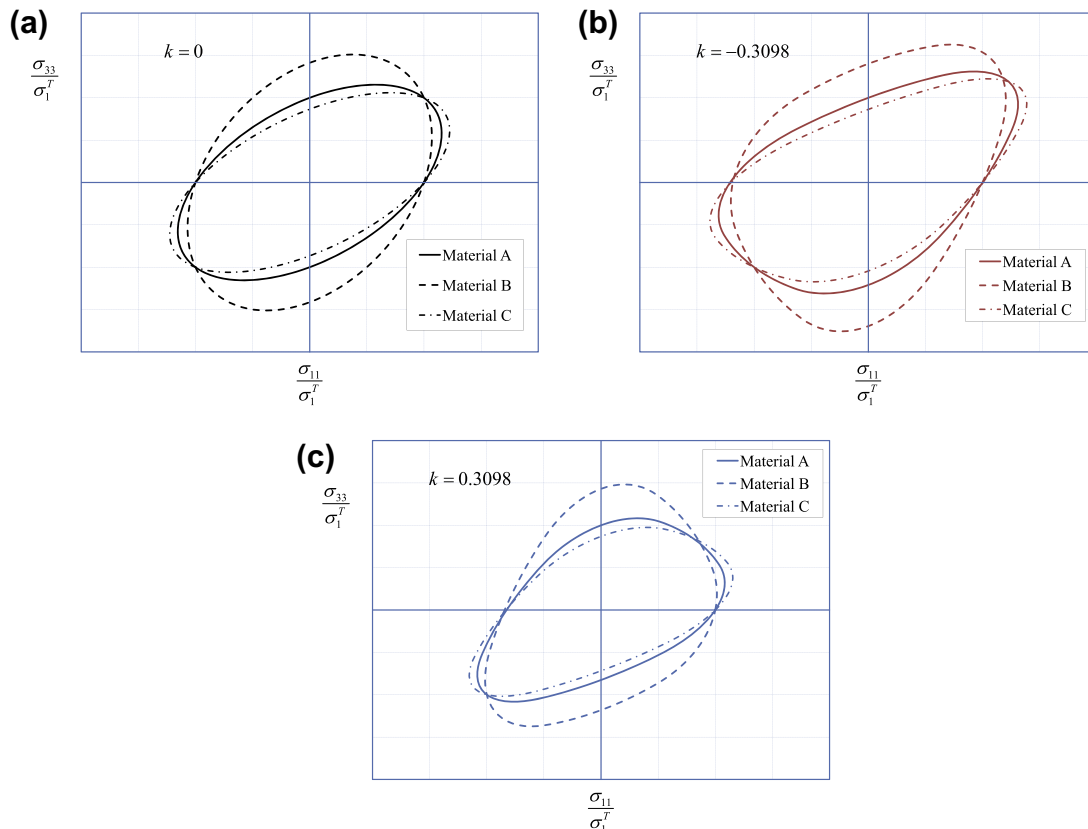

Fig. 2. Plane stress yield loci for void-free materials A (isotropic), B and C (transversely isotropic) according to the CPB06 yield criterion. x is an in-plane direction with z being the through-thickness direction. (a) No strength differential ($k = 0$). (b) Tension–compression asymmetry with the yield strengths in tension less than the yield strengths in compression ($k = -0.3098$). (c) Tension–compression asymmetry with the yield strengths in tension greater than the yield strengths in compression ($k = 0.3098$).

Table 1
Numerical values of the anisotropy coefficients for the materials A, B, and C.

CPB06 parameters	Material A	Material B	Material C
$L_{11} = L_{22}$	1.000	1.054	0.963
L_{33}	1.000	0.850	1.064
$L_{13} = L_{23} = \frac{1}{2}(1 - L_{33})$	0.000	0.075	−0.032
$L_{12} = \frac{1}{2}(1 + L_{33}) - L_{11}$	0.000	−0.129	0.069
L_{44}	1.000	0.775	1.817

sheet, respectively. This choice of anisotropic coefficients serves two purposes: (a) it allows partial verification of the FE implementation of the model (Eq. (68)) and (b) it provides FE data for assessing the analytic yield loci according to Benzerga and Besson (2001) for $k = 0$ and according to Eq. (68) for $k \neq 0$.

For axisymmetric loadings, the effective stress according to the CPB06 anisotropic criterion is related to the von Mises effective stress by the relation

$$\Sigma_e = |\Sigma_{11} - \Sigma_{33}| = g\tilde{\Sigma}_e, \tag{74}$$

where

$$g = \begin{cases} \dfrac{1}{\hat{m}|\Phi_3|\sqrt{2(3k^2 + 2k + 3)}} & \text{for } \Sigma_{11} > \Sigma_{33}, \\ \dfrac{1}{\hat{m}|\Phi_3|\sqrt{2(3k^2 - 2k + 3)}} & \text{for } \Sigma_{11} < \Sigma_{33}. \end{cases} \tag{75}$$

In Fig. 3 are presented the projections of the analytical yield loci given by Eq. (68) in the plane (Σ_e, Σ_m) for a transversely isotropic material of type B with either yield strengths in tension greater than in compression ($k = 0.3098$) or yield strengths in tension less than in compression ($k = -0.3098$).

Note that the effect of the sign of the third invariant of the stress deviator is well captured. Specifically, for purely deviatoric loading, if $\Sigma_{33} > \Sigma_{11}$ then the material yields at

$$\Sigma_e = \frac{\sigma_1^T(1 - f)}{\hat{m}|\Phi_3|\sqrt{2(3k^2 - 2k + 3)}}, \tag{76}$$

whereas for $\Sigma_{33} < \Sigma_{11}$,
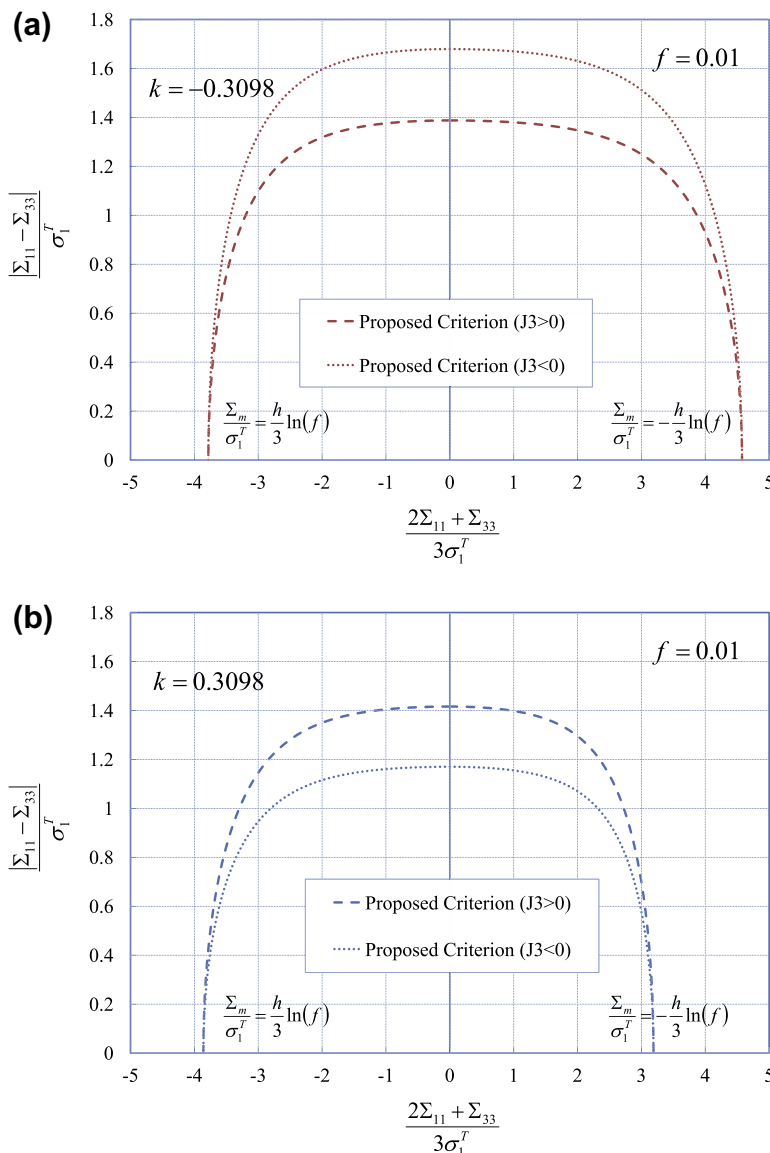
Fig. 3. Anisotropic yield surfaces for a matrix material containing a spherical void of porosity $f = 0.01$ and with the through-thickness yield strength greater than the in-plane yield strength (i.e., material B). (a) Tension–compression asymmetry with the yield strengths in tension less than the yield strengths in compression ($k = -0.3098$). (b) Tension–compression asymmetry with the yield strengths in tension greater than the yield strengths in compression ($k = 0.3098$).

$$\Sigma_e = \frac{\sigma_1^T(1-f)}{\hat{m}|\Phi_3|\sqrt{2(3k^2+2k+3)}},$$ (77)

where, for transverse isotropy,

$$\Phi_3 = \frac{1}{6}(1 - 3L_{33}).$$ (78)

Note also that the yield locus is no longer symmetric with the vertical axis $\Sigma_m = 0$ since h depends on the sign of the mean stress (Eq. (65)). For transverse isotropy, h can be written as

$$h = \sqrt{\frac{6}{15}\hat{n}\left(7\hat{l}_1 + 2\hat{l}_3 + 6\hat{l}_4\right)}.$$ (79)

The effect of the magnitude of the third invariant of the stress deviator can be best assessed through examination of the projections of the yield locus (Eq. (68)) in the π-plane (the plane normal to the hydrostatic axis: $(\mathbf{e}_1 + \mathbf{e}_2 + \mathbf{e}_3)/\sqrt{3}$). Contours corresponding to a porosity of $f = 0.01$ and fixed values of the mean stress $\Sigma_m = 0, 0.75p_Y^+,$ and $0.9p_Y^+$ are plotted in Figs. 4–6 for the six materials considered.

Fig. 4(a)–(c) shows the π-plane representation of the yield loci for a porous aggregate with an isotropic matrix (material type A)

displaying tension–compression asymmetry with $k = 0.3098$ and $k = -0.3098$, along with the von Mises matrix ($k = 0$) for comparison. The effect of the third invariant of the stress deviator is evident in the change in shape of the yield loci from circles to rounded triangles. The combined effects of anisotropy and tension–compression asymmetry are evident from Fig. 5 (material type B) and Fig. 6 (material type C). A very drastic departure of the yield loci from the ellipse ($k = 0$) is observed for both material types B and C.

Fig. 7 shows the π-plane representation of the ductile criterion given by Eq. (68). Fig. 7(a) illustrates the π-plane representation for a von Mises material (material type A with $k = 0$ and $f = 0$). Figs. 7(b)–(d) shows representations with non-zero porosity ($f = 0.01$) for materials of type B with no strength–differential ($k = 0$), yield strength in tension greater than in compression ($k > 0$) and yield strength in tension less than in compression ($k < 0$), respectively. Notice that if there are no voids present (see Fig. 7(a)), the response is independent of the hydrostatic pressure; this is because the matrix material is incompressible. When voids are present, as in Fig. 7(b)–(d), the yield surface shrinks in the deviatoric plane as the pressure increases toward either the tensile or compressive hydrostatic limit pressure (i.e., toward either vertex). Fig. 7 implies that the anisotropy and tension–compression asymmetry of the
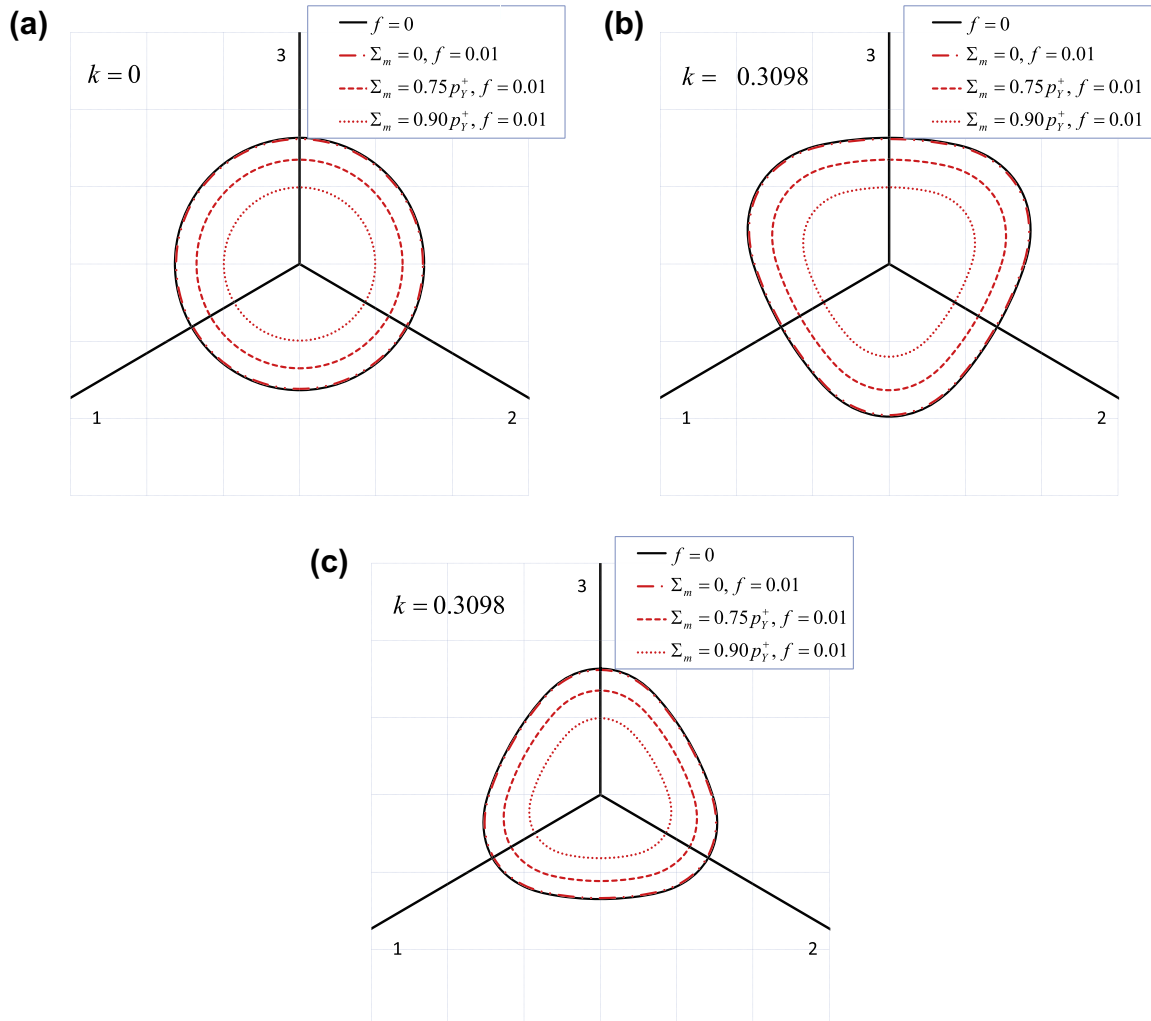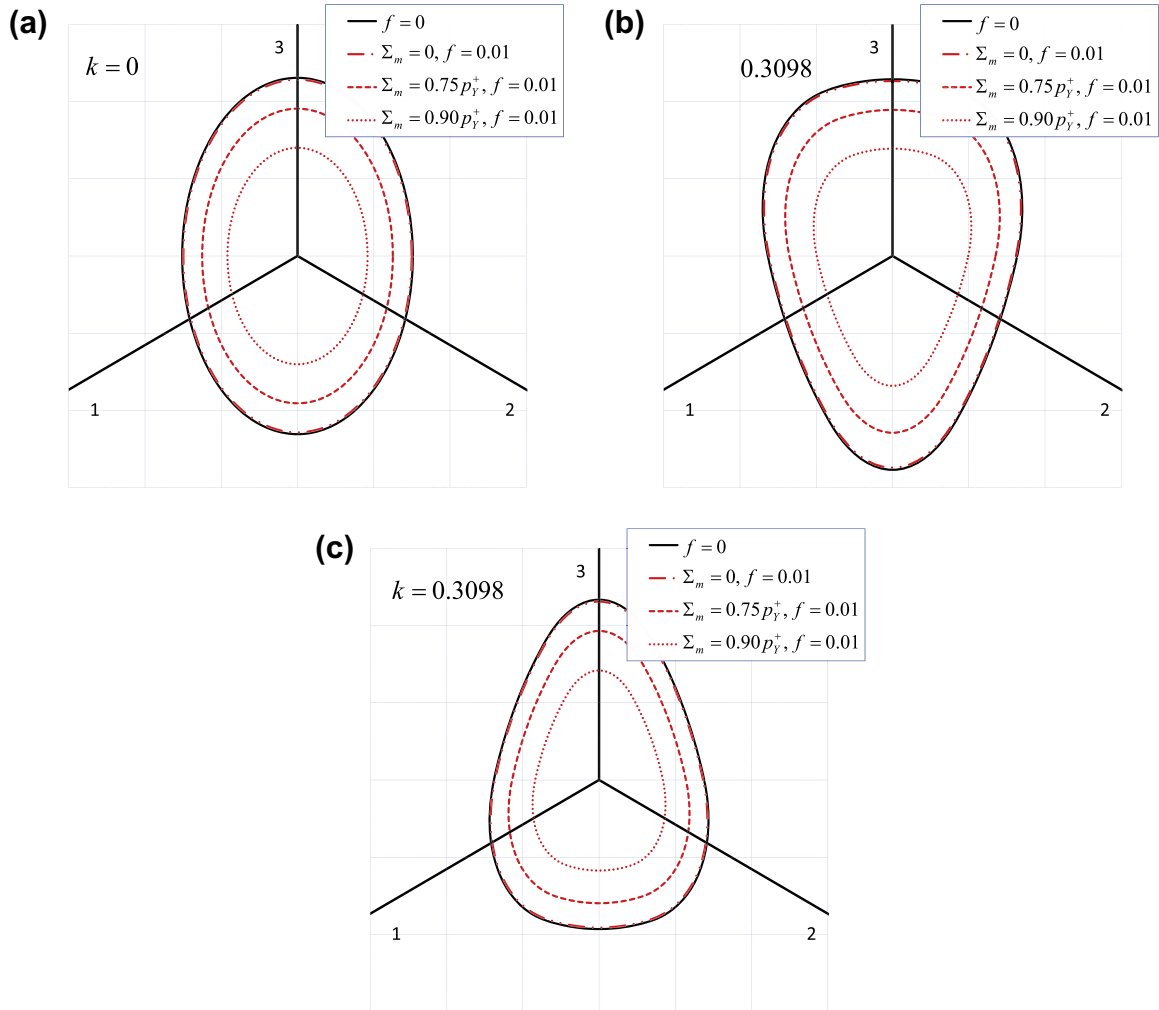

Fig. 4. Representation in the deviatoric plane of the ductile yield criterion given by Eq. (68) for an isotropic material (material A in Table 1). p_Y^+ is the tensile hydrostatic yield pressure. (a) No strength differential ($k = 0$). (b) Tension–compression asymmetry with the yield strengths in tension less than the yield strengths in compression ($k = -0.3098$). (c) Tension–compression asymmetry with the yield strengths in tension greater than the yield strengths in compression ($k = 0.3098$).

Fig. 5. Representation in the deviatoric plane of the ductile yield criterion given by Eq. (68) for a material with the through-thickness yield strength greater than the in-plane yield strength (material *B* in Table 1). p_Y^+ is the tensile hydrostatic yield pressure. (a) No strength differential ($k = 0$). (b) Tension–compression asymmetry with the yield strengths in tension less than the yield strengths in compression ($k = -0.3098$). (c) Tension–compression asymmetry with the yield strengths in tension greater than the yield strengths in compression ($k = 0.3098$).

matrix influences the shape of the yield locus in the deviatoric plane while the presence of voids in the aggregate leads to a decrease in the size of the yield locus with increasing pressure (positive or negative). Fig. 7(b)–(d) show yield surfaces corresponding to a fixed value of the porosity, $f = 0.01$; varying the porosity will simply change the size of the yield locus (the yield locus decreases in size with increasing porosity for a fixed pressure). The shape of the yield locus is governed by the matrix anisotropy and tension–compression asymmetry.

6.2. Validation through finite element cell calculations

The assumption of in-plane isotropy allows axisymmetric calculations to be performed and the results can be used to examine directional effects and the influence of tension–compression asymmetry on yielding. Thus, loading paths of the type ($\Sigma_{11}, \Sigma_{11}, \Sigma_{33}$) will be considered, with $\mathbf{e}_3$ being normal to the plane of isotropy. Tension–compression asymmetry in the matrix due to the combined effects of the matrix asymmetry and the presence of the voids will be assessed by carrying out calculations for both compressive ($\Sigma_m < 0$) and tensile ($\Sigma_m > 0$) axisymmetric loadings.

The axisymmetric unit cell calculations that were carried out are similar to those of Koplik and Needleman (1988), Ristinmaa

(1997) and Cazacu and Stewart (2009) in the sense that the continuum is considered to consist of a periodic assemblage of hexagonal cylindrical unit cells which are approximated by right circular cylinders. Due to symmetry, only one quarter of the unit cell for the anisotropic material is shown in Fig. 8. In the figure, the X_3-axis denotes the through-thickness direction while the X_1-axis is in the plane of isotropy. Every cell of initial length L_0 and radius R_0 contains a spherical void of initial radius a_0 and is subject to homogeneous radial and axial displacements. In other words, the boundary conditions for this unit cell are as follows:

$$u_1 = ur_2 = ur_3 = 0 \quad \text{for} \quad X_1 = 0,$$
$$u_3 = ur_1 = ur_2 = 0 \quad \text{for} \quad X_3 = 0,$$
$$u_1 = U_1 \quad \text{for} \quad X_1 = R,$$
$$u_3 = U_3 \quad \text{for} \quad X_3 = L/2,$$

(80)

where u_i are the displacements in the X_i directions and ur_i are the rotations about the X_i axes. The void is considered to be traction free. Thus, for this axisymmetric unit cell, the initial porosity f_0 is defined as

$$f_0 = \frac{4a_0^3}{3R_0^2 L_0}.$$

(81)
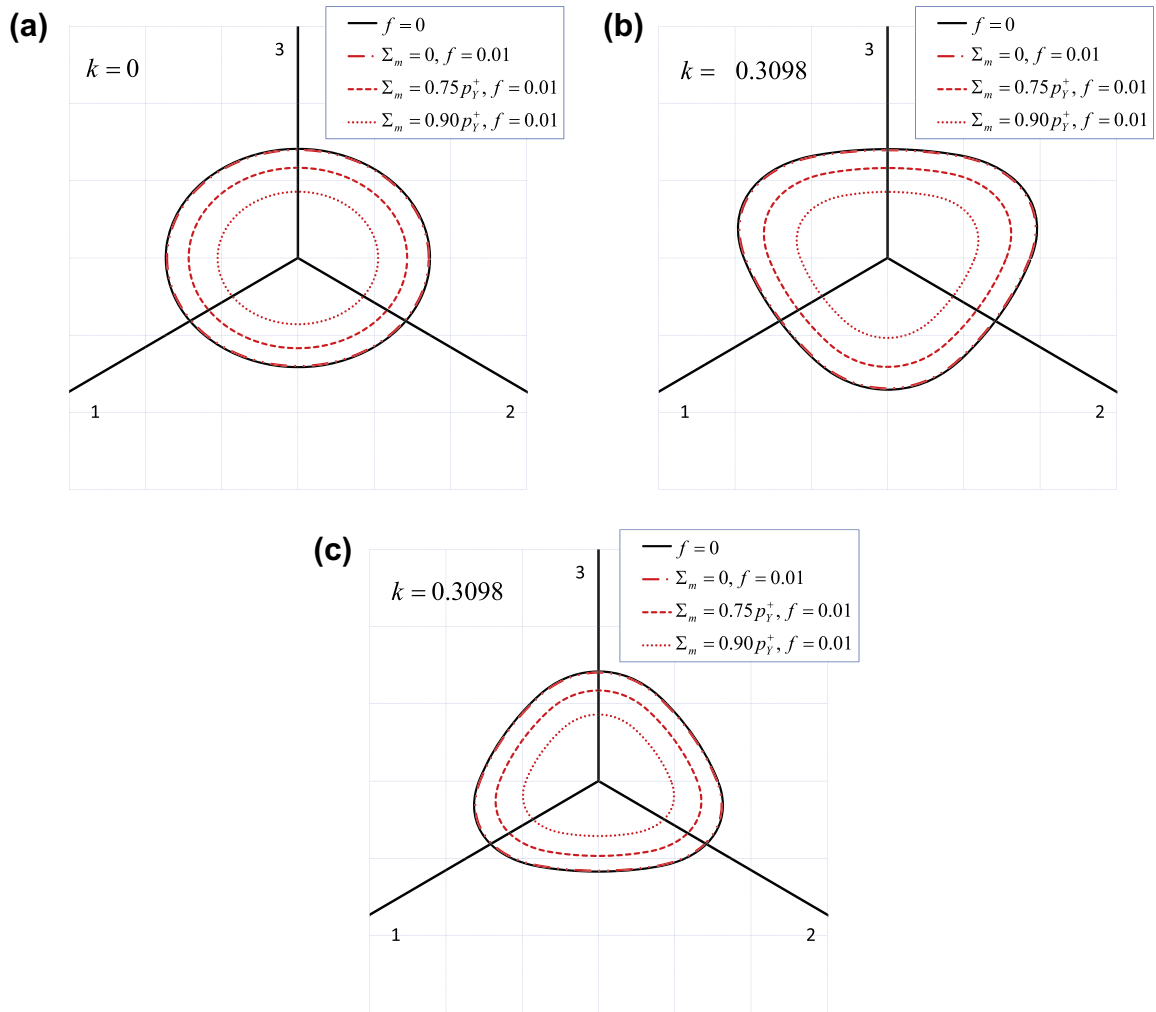
Fig. 6. Representation in the deviatoric plane of the ductile yield criterion given by Eq. (68) for a material with the through-thickness yield strength less than the in-plane yield strength (material C in Table 1). p_Y^+ is the tensile hydrostatic yield pressure. (a) No strength differential ($k = 0$). (b) Tension–compression asymmetry with the yield strengths in tension less than the yield strengths in compression ($k = -0.3098$). (c) Tension–compression asymmetry with the yield strengths in tension greater than the yield strengths in compression ($k = 0.3098$).

The macroscopic principal strains, the effective von Mises macroscopic strain E_e and the strain triaxiality T_E are defined as follows:

$$E_{11} = \ln\left(\frac{R}{R_0}\right) = \ln\left(\frac{R_0 + U_1}{R_0}\right),$$
$$E_{33} = \ln\left(\frac{L}{L_0}\right) = \ln\left(\frac{L_0 + 2U_3}{L_0}\right), \tag{82}$$

$$E_e = \sqrt{\frac{2}{3} E'_{ij} E'_{ij}} \tag{83}$$

and

$$T_E = \frac{E_{kk}}{3E_e} = \frac{2E_{11} + E_{33}}{2|E_{11} - E_{33}|}, \tag{84}$$

where E_{kk} is the trace of the macroscopic strain tensor and E'_{ij} are the components of the macroscopic deviatoric strain tensor.

The macroscopic stress $\boldsymbol{\Sigma}$ is also axisymmetric such that

$$\Sigma_{11} = \Sigma_{22} = \frac{F_1}{\pi R L},$$
$$\Sigma_{33} = \frac{F_3}{\pi R^2}, \tag{85}$$

where F_1 is the total radial force at $X_1 = R$ and F_3 is the total axial force at $X_3 = L/2$. Due to axisymmetric loading, $J_3^\Sigma = -(2/27)(\Sigma_{11} - \Sigma_{33})^3$; thus, only the effect of the sign of the third invariant can be examined in the current analysis.

The analytical yield criterion of Eq. (68) can be modified to include additional parameters, q_i, as was done by Tvergaard (1981) and Tvergaard and Needleman (1984) in the case of Gurson's (1977) yield criterion as follows:

$$\Phi = \left(\frac{\tilde{\Sigma}_e}{\sigma_1^T}\right)^2 + 2q_1 f \cosh\left(\frac{3q_2 \Sigma_m}{h\sigma_1^T}\right) - 1 - q_3 f^2, \tag{86}$$

where values of $q_1 = 4/e$, $q_2 = 1$ and $q_3 = q_1^2$ will be used in the following (these values were suggested in Leblond and Perrin, 1990, based on an analysis of the effects of a second population of small voids on the growth of a large void). In the next section, the analytical yield surfaces given by Eq. (86) will be compared to data from finite element unit cell calculations.

6.3. Results

All calculations were performed assuming elastic, ideal-plastic behavior for the matrix with the plastic potential given by the CPB06 anisotropic criterion (see Eq. (47)). A user material
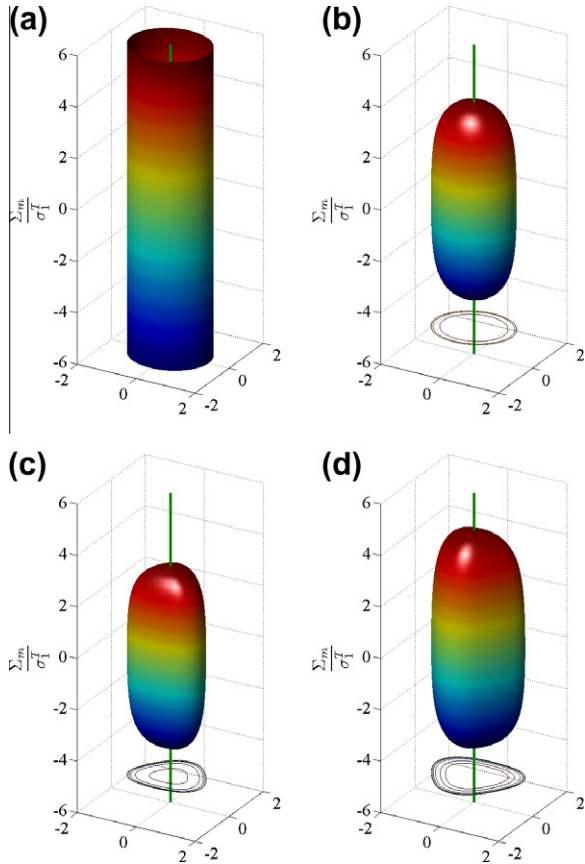
Fig. 7. Representation in the deviatoric plane of the ductile yield criterion given by Eq. (68) for a material with the through-thickness yield strength greater than the in-plane yield strength (material type B in Table 1). (a) No tension–compression asymmetry ($k = 0$) and no voids ($f = 0$). (b) No tension–compression asymmetry with $f = 0.01$. (c) Yield strengths in tension greater than in compression ($k = 0.3098$) with $f = 0.01$. (d) Yield strengths in tension less than in compression ($k = -0.3098$) with $f = 0.01$.
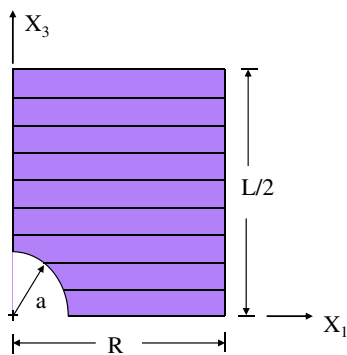
Fig. 8. Quarter section of the unit cell for transversely isotropic materials containing spherical voids; axis X_3 is the axis of rotational symmetry with the X_1–X_2 plane being the plane of symmetry.

subroutine was written for the commercial FE program ABAQUS (see Abaqus, 2008) using a fully implicit return mapping algorithm. A mesh refinement study was performed using four-node quadri-lateral elements (with reduced integration and ABAQUS' enhanced hourglass control) to ensure solution convergence. Fig. 9 shows the mesh used for all tests. The matrix elastic properties are $E/\sigma_1^T = 800$ and $v = 0.32$, where E is the Young's modulus and v is the Poisson's ratio. For ease of comparison, the tensile yield strength in the
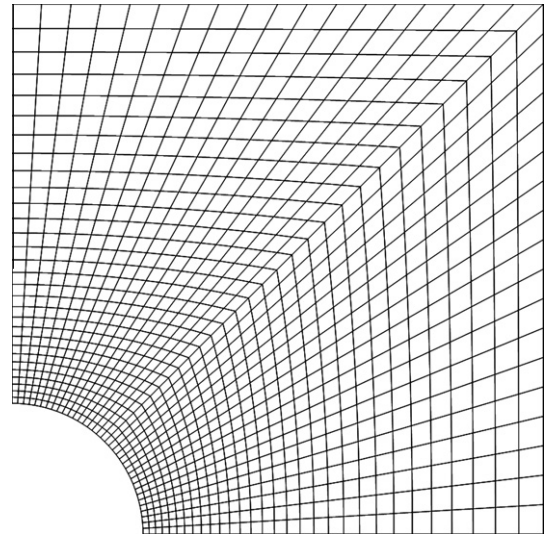
**Fig. 9.** $f_0 = 0.01$ axisymmetric finite element mesh for the unit cell.

$\mathbf{e}_1$ direction, σ_1^T, was considered to be the same for all material types A, B, and C.

The model implementation was first verified by performing calculations corresponding to $k = 0$ for material type A (isotropic) and transversely isotropic (B and C), which correspond to a von Mises matrix (for material type A) and Hill matrices (for material types B and C), and comparing the results to those obtained using the ABAQUS built-in von Mises and Hill material models for the matrix. As an example, in Fig. 10 are shown the results of these FE calculations in terms of the von Mises effective stress Σ_e versus the von Mises effective strain E_e for each material. In the calculations illustrated in Fig. 10, the displacements were prescribed such that a constant value of the strain triaxiality ($T_E = 1.5$) was maintained and the major stress was oriented along the $\mathbf{e}_3$ direction ($\Sigma_{33} > \Sigma_{11} > 0$). Both materials B and C have the same yield strength along the in-plane direction $\mathbf{e}_1$. However, since the matrix in material C is softest in the $\mathbf{e}_3$ direction, there is more plastic flow and, hence, more void growth than in material B, for which the $\mathbf{e}_3$ direction is the hardest. Consequently, material C yields first at at a lower stress level and its overall softening is much more pronounced than in material B. Comparison between the isotropic stress–strain curve and the anisotropic ones illustrate very clearly the effect of the directionality of the plastic flow of the matrix on yielding of the void matrix aggregate. Overall softening in the isotropic material is less pronounced than in material C since, while all three materials have the same yield strength in the $\mathbf{e}_1$ direction, material A has equal yield strengths in the $\mathbf{e}_1$ and $\mathbf{e}_3$ directions whereas material C has a lower yield strength in the $\mathbf{e}_3$ direction.

Figs. 11–13 show the finite element results versus Eq. (86) where three different materials (corresponding to material types A, B and C with $k = 0.3098$ such that the yield strengths in tension are greater than in compression) are each used as the matrix material in a unit cell containing a spherical void (1% void volume fraction). The figures show the normalized macroscopic von Mises effective stress Σ_e/σ_1^T versus the normalized macroscopic mean stress Σ_m/σ_1^T; the numerical values of the anisotropy coefficients are given in Table 1. The macroscopic yield points for the finite element calculations were taken to correspond with the points of maximum macroscopic effective stress. Results corresponding to both positive and negative values of the third invariant of the stress deviator J_3^Σ are reported in the figures.

Fig. 11 shows a comparison between the finite element results versus the theoretical yield curves given by Eq. (86) when the
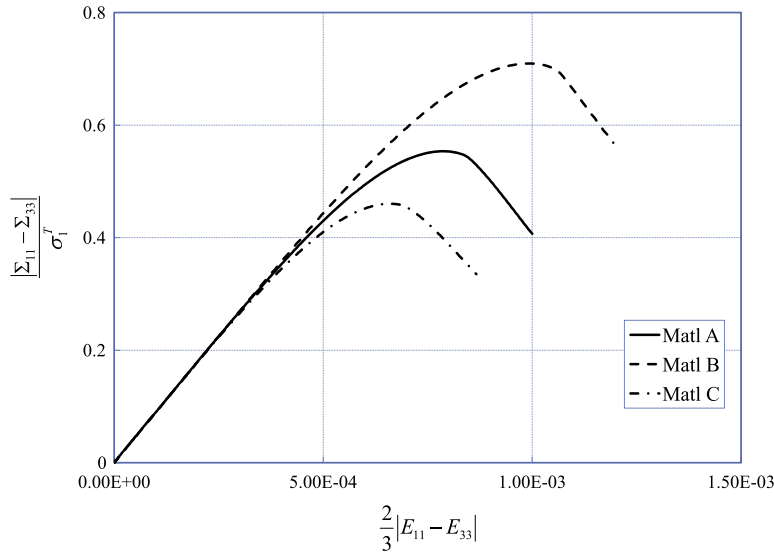
Fig. 10. Typical von Mises effective stress versus von Mises effective strain curves corresponding to FE calculations at T_E = 1.5 and with the major stress in the $\mathbf{e}_3$ direction. For all materials the yield stress in tension and compression are equal ($k = 0$) with material type A being isotropic ($\sigma_1^{T,C} = \sigma_3^{T,C}$), material type B having a through-thickness yield strength greater than the in-plane yield strength ($\sigma_1^{T,C} < \sigma_3^{T,C}$) and material type C having a through-thickness yield strength lower than the in-plane yield strength ($\sigma_1^{T,C} > \sigma_3^{T,C}$).
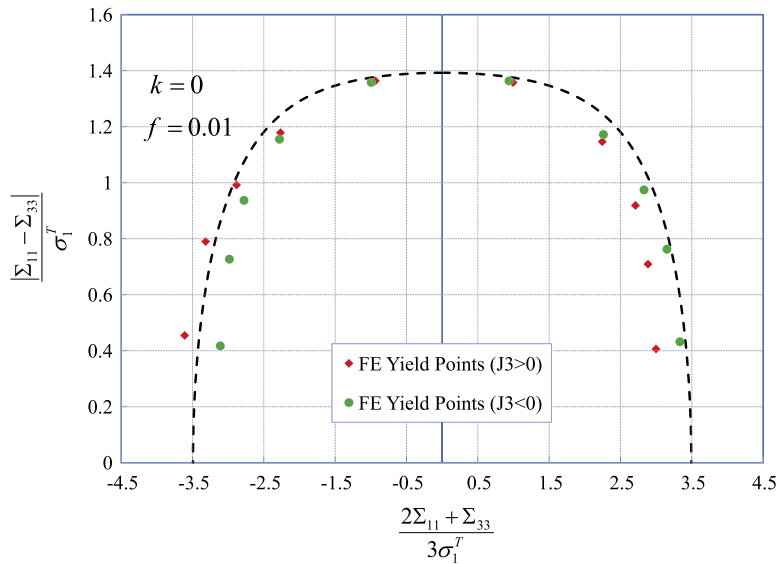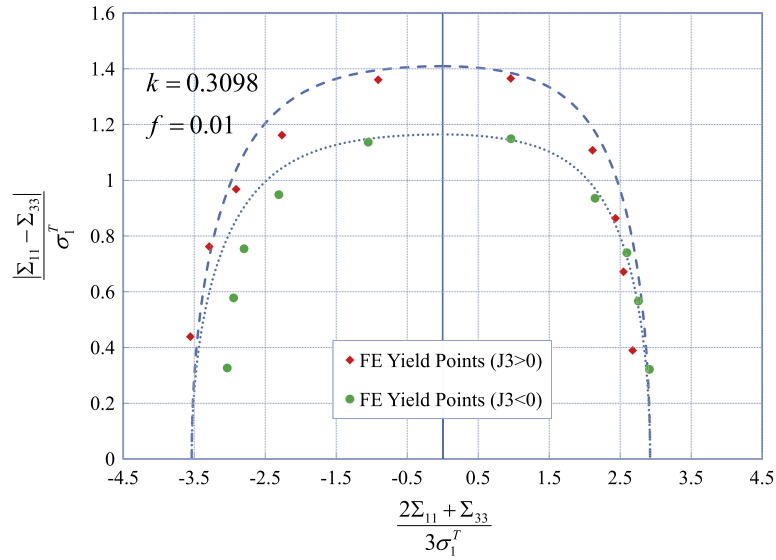

Fig. 11. Analytical yield curves according to the Benzerga and Besson (2001) criterion and axisymmetric FE results corresponding to an anisotropic matrix (i.e., material type B in Table 1 with $k = 0$). The void volume fraction is $f_0 = 0.01$.

matrix materials are anisotropic (the anisotropy coefficients correspond to material type B of Table 1) and does not display tension compression asymmetry ($k = 0$). Thus, Eq. (86) reduces to the analytical criterion of Benzerga and Besson (2001). As in the case of Gurson (1977), the Benzerga and Besson (2001) yield criterion does not account for the effect of the third invariant of the stress deviator; yet, the agreement with FE results is still quite good.

Figs. 12 and 13 show FE results together with the analytical yield curves corresponding to materials having the yield strength in the through-thickness direction greater than the yield strength in any in-plane direction and vice versa, respectively (i.e., materials type B and C, respectively, from Table 1). To examine the combined effects of anisotropy and tension–compression asymmetry, axisymmetric calculations were performed with the through-thickness direction, $\mathbf{e}_3$, corresponding to either the major stress

($J_3^\Sigma > 0$) or to the minor stress ($J_3^\Sigma < 0$). The agreement between the analytical yield curves according to the developed criterion (Eq. (86)) and the finite element results obtained from the unit cell calculations is satisfactory.

Finally, Fig. 14 shows a comparison between the FE results and the anisotropic yield criterion of Eq. (86) for three different materials, each having the through-thickness direction $\mathbf{e}_3$ the hardest but displaying various levels of tension–compression asymmetry ($k = 0$, $k > 0$ and $k < 0$). The FE data corresponds to axisymmetric loading with the minor stress being in the through-thickness direction (i.e., $J_3^\Sigma < 0$). The model accurately predicts that for the same yield strength ratio, the softest material corresponds to $k > 0$ while the hardest corresponds to $k < 0$ (see also Eqs. (70), (71) and (77) which give the expressions of the intercepts of the yield locus with the hydrostatic and deviatoric axes as functions of the strength–

Fig. 12. Analytical yield curves according to the proposed criterion (Eq. (86)) and axisymmetric FE results for both $J_3^\Sigma > 0$ and $J_3^\Sigma < 0$. The anisotropic matrix material is hardest in the through-thickness direction (i.e., material type B in Table 1) and displays tension–compression asymmetry with the tensile yield strengths larger than the compressive ones ($k = 0.3098$). The void volume fraction is $f_0 = 0.01$.
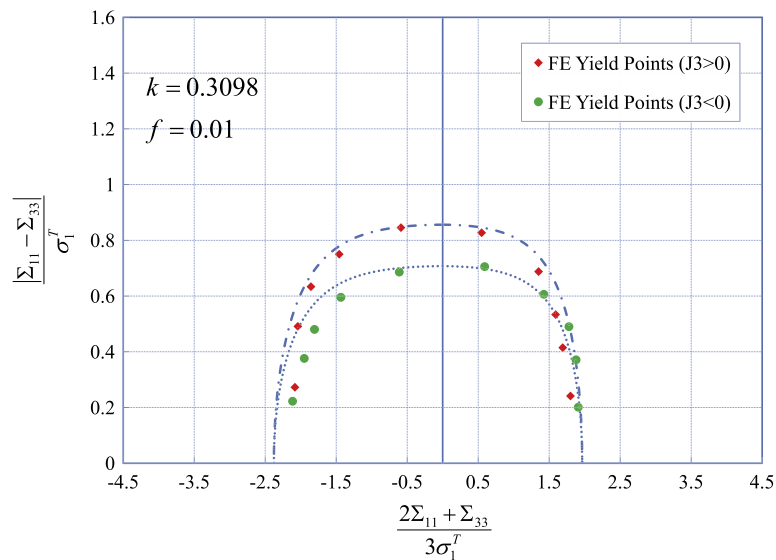
Fig. 13. Analytical yield curves according to the proposed criterion (Eq. (86)) and axisymmetric FE results for both $J_3^\Sigma > 0$ and $J_3^\Sigma < 0$. The anisotropic matrix material is softest in the through-thickness direction (i.e., material type C in Table 1) and displays tension–compression asymmetry with the tensile yield strengths larger than the compressive ones ($k = 0.3098$). The void volume fraction is $f_0 = 0.01$.

differential parameter k). Once again, the comparison between finite element data and the yield curves shows quite good agreement.

7. Concluding remarks

Yielding of porous materials in which the matrix is incompressible, anisotropic, and displays tension–compression asymmetry has been studied. An analytical yield criterion has been developed by extending Gurson's (1977) analysis of the hollow sphere to the case when the matrix plastic behavior is described by the anisotropic yield criterion of Cazacu et al. (2006). The classical velocity field of Rice and Tracey (1969) has been used in the upper bound calculations. This velocity field is the simplest among the fields that meet the requirements of the Hill–Mandel lemma, i.e., incom-

pressibility and compatibility with uniform strain rate boundary conditions. There are several studies that motivate the examination of more complex microscopic flow fields (e.g., Needleman, 1972; Koplik and Needleman, 1988). Specifically, it is shown that part of the matrix might not attain plastic yield and that elastic unloading may occur in certain subdomains. Nevertheless, even using the simplest velocity field, fresh difficulties were encountered when estimating the local plastic dissipation associated with the Cazacu et al. (2006) yield criterion. These difficulties are related to the tension–compression asymmetry and anisotropy of the matrix response. Thus, the plastic multiplier rate has multiple branches (see Eq. (28)) and depends on each of the principal values of the local rate of deformation, **d**.

Certain approximations were introduced in order to obtain the analytical, closed-form expression of the overall plastic potential (Eq. (68)). The derived criterion is anisotropic, exhibits tension–
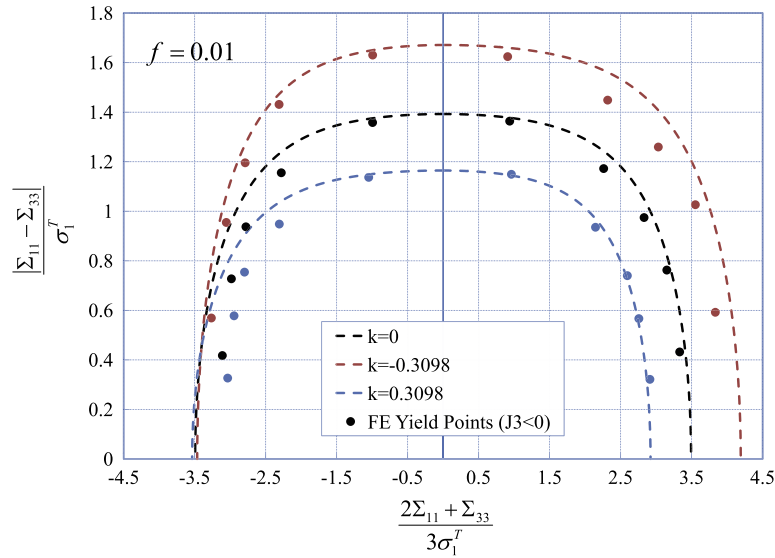
Fig. 14. Anisotropic, axisymmetric finite element yield points versus analytic curves when the initial void volume fraction is $f_0 = 0.01$ and the matrix material is hardest in the through-thickness direction (i.e., material type *B* in Table 1). The curves shown are for $k = 0$ (no strength differential), $k = 0.3098$ (yield strengths in tension greater than in compression) and $k = -0.3098$ (yield strengths in tension less than in compression) with $\Sigma_{33} < \Sigma_{11}$.

compression asymmetry due to the characteristics of the plastic flow of the matrix and is pressure-sensitive due to the presence of voids. It is worth noting that this criterion depends on all stress invariants as well as the mixed invariants between stress and structural tensors. Comparison between the theoretical predictions using this criterion and results of finite element cell calculations show an overall good agreement.

Although the expression of the proposed criterion for the porous material is similar to that of Benzerga and Besson (2001), there are distinct differences.

- The Hill (1948) equivalent stress is replaced by $\tilde{\Sigma}_e = \hat{m}\sqrt{\sum_{i=1}^{3}(|\hat{\Sigma}_i| - k\hat{\Sigma}_i)^2}$, the equivalent stress associated to the CPB06 anisotropic criterion, which depends on all principal values of the stress deviator $\mathbf{\Sigma}'$, the anisotropy coefficients L_{ij} and on the ratio between the uniaxial yield in tension σ_1^T and the uniaxial yield in compression σ_1^C of the matrix through the parameter $\hat{m}$ (see Eq. (16) for the definition of the constant $\hat{m}$).
- It involves a new coefficient h such that for tensile hydrostatic loading, yielding of the void-matrix aggregate occurs when $\Sigma_m = -\sigma_1^T \sqrt{\frac{2}{15\hat{m}^2}\left(\frac{7\hat{l}_1+2\hat{l}_3+6\hat{l}_4}{3k^2+2k+3}\right)}\ln(f)$ while for compressive hydrostatic loading yielding is at $\Sigma_m = \sigma_1^T \sqrt{\frac{2}{15\hat{m}^2}\left(\frac{7\hat{l}_1+2\hat{l}_3+6\hat{l}_4}{3k^2-2k+3}\right)}\ln(f)$. Thus, for arbitrary loadings the effective yield locus is no longer symmetric with respect to the vertical axis $\Sigma_m = 0$, as it is in the case of Gurson (1977) or Benzerga and Besson's (2001) yield locus.

If there is no difference in response between the yield in tension and compression, $\tilde{\Sigma}_e$ reduces to Hill's equivalent stress and the coefficient h reduces to the expression

$$h = \sqrt{(8/15)(\hat{l}_1 + \hat{l}_2 + \hat{l}_3) + (4/5)(\hat{l}_4 + \hat{l}_5 + \hat{l}_6)}, \qquad (87)$$

which coincides with the hydrostatic factor in Benzerga and Besson's (2001) criterion (since for $k = 0$, the quadratic form of Cazacu et al.'s (2006) anisotropic criterion reduces to Hill's (1948) anisotropic criterion); hence, the proposed criterion (Eq. (68)) reduces to the criterion of Benzerga and Besson (2001). In the absence of voids, the proposed criterion reduces to Cazacu et al.'s (2006) anisotropic yield criterion. The accuracy of the analytical criterion was

assessed through comparison with finite-element cell calculations. To improve the agreement, the proposed analytic yield criterion (Eq. (68)) was modified to include additional parameters, q_i, as done by Tvergaard (1981), Tvergaard and Needleman (1984) in the case of the Gurson (1977) yield criterion. In this manner, for $k = 0$ and $\mathbf{L} = \mathbf{1}$ (a von Mises matrix), the criterion reduces to the GTN model, while for k non-zero and $\mathbf{L}$ isotropic it reduces to Cazacu and Stewart (2009). The agreement between the theoretical predictions using this criterion (Eq. (86)) and the results of finite element cell calculations are quite good.

Appendix A. Calculation of the hydrostatic parameter

The hydrostatic parameter, h, is given as

$$h^2 = \hat{n}\langle\bar{\mathbf{d}} : \hat{\mathbf{L}} : \bar{\mathbf{d}}\rangle_{S(r)} = \frac{\hat{n}}{4\pi}\int_0^{2\pi}\int_0^{\pi}\left(\bar{\mathbf{d}} : \hat{\mathbf{L}} : \bar{\mathbf{d}}\right)\sin\theta d\theta d\phi, \qquad (88)$$

where

$$\bar{\mathbf{d}} = -2\mathbf{e}_r \otimes \mathbf{e}_r + \mathbf{e}_\theta \otimes \mathbf{e}_\theta + \mathbf{e}_\phi \otimes \mathbf{e}_\phi. \qquad (89)$$

The basis vectors for the spherical coordinate system ($\mathbf{e}_r, \mathbf{e}_\theta, \mathbf{e}_\phi$) are expressed in terms of the basis vectors for the Cartesian coordinate system associated with the material axes of symmetry ($\mathbf{e}_1, \mathbf{e}_2, \mathbf{e}_3$) as follows:

$$\begin{aligned}\mathbf{e}_r &= (\sin\theta\cos\phi)\mathbf{e}_1 + (\sin\theta\sin\phi)\mathbf{e}_2 + \cos\theta\mathbf{e}_3, \\ \mathbf{e}_\theta &= (\cos\theta\cos\phi)\mathbf{e}_1 + (\cos\theta\sin\phi)\mathbf{e}_2 - \sin\theta\mathbf{e}_3, \\ \mathbf{e}_\phi &= -\sin\phi\mathbf{e}_1 + \cos\phi\mathbf{e}_2,\end{aligned} \qquad (90)$$

where $\theta \in [0, \pi]$ and $\phi \in [0, 2\pi]$.

In order to evaluate the integral expression in Eq. (88), the tensor $\bar{\mathbf{d}}$ will be transformed from the spherical coordinate system to the material coordinate system. Thus,

$$\bar{\mathbf{d}}_{(1,2,3)} = \mathbf{R}\bar{\mathbf{d}}_{(r,\theta,\phi)}\mathbf{R}^T, \tag{91}$$

where

$$\mathbf{R} = \begin{bmatrix} \cos\phi\sin\theta & \cos\phi\cos\theta & -\sin\phi \\ \sin\phi\sin\theta & \sin\phi\cos\theta & \cos\phi \\ \cos\theta & -\sin\theta & 0 \end{bmatrix} \tag{92}$$

such that

$$\bar{\mathbf{d}}_{(1,2,3)} = \begin{bmatrix} 1-3\sin^2\theta\cos^2\phi & -3\sin^2\theta\sin\phi\cos\phi & -3\sin\theta\cos\theta\cos\phi \\ -3\sin^2\theta\sin\phi\cos\phi & 1-3\sin^2\theta\sin^2\phi & -3\sin\theta\cos\theta\sin\phi \\ -3\sin\theta\cos\theta\cos\phi & -3\sin\theta\cos\theta\sin\phi & 1-3\cos^2\theta \end{bmatrix}. \tag{93}$$

Note that

$$\bar{\mathbf{d}} : \widehat{\mathbf{L}} : \bar{\mathbf{d}} = \hat{l}_1\bar{d}_{11}^2 + \hat{l}_2\bar{d}_{22}^2 + \hat{l}_3\bar{d}_{33}^2 + 2\left(\hat{l}_4\bar{d}_{23}^2 + \hat{l}_5\bar{d}_{13}^2 + \hat{l}_6\bar{d}_{12}^2\right). \tag{94}$$

Therefore, evaluating the integral expression in Eq. (88) reduces to evaluating the surface integral of the squared components of $\bar{\mathbf{d}}_{(1,2,3)}$. Referring to Eq. (93) yields

$$\langle\bar{d}_{11}^2\rangle_{S(r)} = \langle\bar{d}_{22}^2\rangle_{S(r)} = \langle\bar{d}_{33}^2\rangle_{S(r)} = \frac{4}{5},$$
$$\langle\bar{d}_{23}^2\rangle_{S(r)} = \langle\bar{d}_{13}^2\rangle_{S(r)} = \langle\bar{d}_{12}^2\rangle_{S(r)} = \frac{3}{5}. \tag{95}$$

Finally, an expression for the hydrostatic parameter, h, is arrived at by combining Eqs. (88), (94) and (95). Thus,

$$h^2 = \hat{n}\left[\frac{4}{5}\left(\hat{l}_1 + \hat{l}_2 + \hat{l}_3\right) + \frac{6}{5}\left(\hat{l}_4 + \hat{l}_5 + \hat{l}_6\right)\right]. \tag{96}$$

References

Abaqus, 2008. Abaqus Analysis User's Manual, Version 6.8, Volumes I–V. Dassault Systèmes Simulia Corp., Providence, RI.

Benzerga, A.A., Besson, J., 2001. Plastic potentials for anisotropic porous solids. European Journal of Mechanics A/Solids 20, 397–434.

Benzerga, A.A., Besson, J., Pineau, A., 2004a. Anisotropic ductile fracture. Part I: Experiments. Acta Materialia 52, 4623–4638.

Benzerga, A.A., Besson, J., Pineau, A., 2004b. Anisotropic ductile fracture. Part II: Theory. Acta Materialia 52, 4639–4650.

Brunet, M., Morestin, F., Walter, H., 2004. Damage identification for anisotropic sheet-metals using a non-local damage model. International Journal of Damage Mechanics 13 (1), 35–57.

Cazacu, O., Ionescu, I.R., Yoon, J.W., 2010. Orthotropic strain rate potential for description of tension–compression asymmetry in hexagonal materials. International Journal of Plasticity 26, 887–904.

Cazacu, O., Plunkett, B., Barlat, F., 2006. Orthotropic yield criterion for hexagonal closed packed metals. International Journal of Plasticity 22, 1171–1194.

Cazacu, O., Stewart, J.B., 2009. Analytic plastic potential for porous aggregates with matrix exhibiting tension–compression asymmetry. Journal of the Mechanics and Physics of Solids 57, 325–341.

Chien, W.Y., Pan, J., Tang, S.C., 2001. Modified anisotropic Gurson yield criterion for porous ductile sheet metals. Journal of Engineering Materials and Technology 123, 409–413.

Cuitiño, A.M., Ortiz, M., 1996. Ductile fracture by vacancy condensation in f.c.c. single crystals. Acta Metallurgica 44 (2), 427–436.

Garajeu, M., 1995. Contribution à l'étude du comportement non linéaire de milieux poreux avec ou sans renfort. Ph.D. Thesis, University of Marseille, Marseille, France.

Garajeu, M., Michel, J.C., Suquet, P., 2000. A micromechanical approach of damage in viscoplastic materials by evolution in size, shape and distribution of voids. Computer Methods in Applied Mechanics and Engineering 183, 223–246.

Gologanu, M., Leblond, J.-B., Devaux, J., 1993. Approximate models for ductile metals containing non-spherical voids–case of axisymmetric prolate ellipsoidal cavities. Journal of the Mechanics and Physics of Solids 41 (11), 1723–1754.

Gologanu, M., Leblond, J.-B., Devaux, J., 1994. Approximate models for ductile metals containing non-spherical voids – case of axisymmetric oblate ellipsoidal cavities. Journal of Engineering Materials and Technology 116, 290–297.

Gologanu, M., Leblond, J.-B., Perrin, G., Devaux, J., 1997. Recent extensions of gurson's model for porous ductile metals. In: Suquet, P. (Ed.), Continuum Micromechanics. Springer-Verlag, New York, pp. 61–130.

Guo, T.F., Faleskog, J., Shih, C.F., 2008. Continuum modeling of a porous solid with pressure-sensitive dilatant matrix. Journal of the Mechanics and Physics of Solids 56, 2188–2212.

Gurson, A.L., 1977. Continuum theory of ductile rupture by void nucleation and growth: Part I- Yield criteria and flow rules for porous ductile media. Journal of Engineering Materials and Technology 99 (January), 2–15.

Hill, R., 1948. A theory of the yielding and plastic flow of anisotropic metals. Proceedings of the Royal Society of London. Series A, Mathematical and Physical Sciences 193 (1033), 281–297.

Hill, R., 1967. The essential structure of constitutive laws for metal composites and polycrystals. Journal of the Mechanics and Physics of Solids 15, 79–95.

Hill, R., 1987. Constitutive dual potentials in classical plasticity. Journal of the Mechanics and Physics of Solids 35 (1), 23–33.

Hosford, W.F., Allen, T.J., 1973. Twinning and directional slip as a cause for a strength differential effect. Metallurgical Transactions 4, 1424–1425.

Huez, J., Feaugas, X., Helbert, A.L., Guillot, I., Clavel, M., 1998. Damage process in commercially pure α-titanium alloy without (Ti40) and with (Ti40-h) hydrides. Metallurgical and Materials Transactions A 29A (June), 1615–1628.

Jeong, H.-Y., Pan, J., 1995. A macroscopic constitutive law for porous solids with pressure-sensitive matrices and its implications to plastic flow localization. International Journal of Solids and Structures 32 (24), 3669–3691.

Keralavarma, S.M., Benzerga, A.A., 2010. A constitutive model for plastically anisotropic solids with non-spherical voids. Journal of the Mechanics and Physics of Solids 58, 874–901.

Khan, A.S., Kazmi, R., Farrokh, B., 2007. Multiaxial and non-proportional loading responses, anisotropy and modeling of Ti6Al4V titanium alloy over wide ranges of strain rates and temperatures. International Journal of Plasticity 23, 931–950.

Koplik, J., Needleman, A., 1988. Void growth and coalescence in porous plastic solids. International Journal of Solids and Structures 24, 835–853.

Kysar, J.W., Gan, Y.X., 2007. Cylindrical void in a rigid-ideally plastic single crystal III: Hexagonal close-packed crystal. International Journal of Plasticity 23 (4), 592–619.

Kysar, J.W., Gan, Y.X., Mendez-Arzuza, G., 2005. Cylindrical void in a rigid-ideally plastic single crystal. Part I: Anisotropic slip line theory solution for face-centered cubic crystals. International Journal of Plasticity 21 (8), 1481–1520.

Kysar, J.W., Gan, Y.X., Morse, T.L., 2006. Cylindrical void in a rigid-ideally plastic single crystal II: Experiments and simulations. International Journal of Plasticity 22 (1), 39–72.

Leblond, J.-B., 2003. Mécanique de la Rupture Fragile et Ductile. Hermes Science Publications.

Leblond, J.-B., Perrin, G., 1990. Analytical study of a hollow sphere made of plastic porous material and subjected to hydrostatic tension – application to some problems in ductile fracture of metals. International Journal of Plasticity 6, 677–699.

Liao, K.C., Pan, J., Tang, S.C., 1997. Approximate yield criteria for anisotropic porous ductile sheet metals. Mechanics of Materials 26, 213–226.

Lubarda, V.A., Schneider, M.S., Kalantar, D.H., Remington, B.A., Meyers, M.A., 2004. Void growth by dislocation emission. Acta Materialia 52, 1397–1408.

Mandel, J., 1972. Plasticité classique et viscoplasticité. CISM courses and lectures. International Centre for Mechanical Sciences, vol. 97. Springer-Verlag, Wien-New York.

McClintock, F.A., 1968. A criterion for ductile fracture by the growth of holes. Journal of Applied Mechanics (June), 363–371.

Monchiet, V., Cazacu, O., Charkaluk, E., Kondo, D., 2008. Macroscopic yield criteria for plastic anisotropic materials containing spheroidal voids. International Journal of Plasticity 24, 1158–1189.

Needleman, A., 1972. Void growth in an elastic plastic medium. Journal of Applied Mechanics 39, 964–970.

Nixon, M.E., 2008. Experimental Characterization and Modeling of the Mechanical Response of Titanium for Quasi-static and High Strain Rate Loads. Ph.D. Thesis, University of Florida, Gainesville, FL.

Plunkett, B., Cazacu, O., Barlat, F., 2008. Orthotropic yield criteria for description of the anisotropy in tension and compression of sheet metals. International Journal of Plasticity 24, 847–866.

Rice, J.R., Tracey, D.M., 1969. On the ductile enlargement of voids in triaxial stress fields. Journal of the Mechanics and Physics of Solids 17, 201–217.

Ristinmaa, M., 1997. Void growth in cyclic loaded porous plastic solid. Mechanics of Materials 26, 227–245.

Rousselier, G., 1987. Ductile fracture models and their potential in local approach of fracture. Nuclear Engineering and Design 105, 97–111.

Tomé, C.N., Maudlin, P.J., Lebensohn, R.A., Kaschner, G.C., 2001. Mechanical response of zirconium – I. Derivation of a polycrystal constitutive law and finite element analysis. Acta Materialia 49, 3085–3096.

Tvergaard, V., 1981. Influence of voids on shear band instabilities under plane strain conditions. International Journal of Fracture 17 (4), 389–407.

Tvergaard, V., Needleman, A., 1984. Analysis of the cup-cone fracture in a round tensile bar. Acta Metallurgica 32 (1), 157–169.

Vitek, V., Mrovec, M., Bassani, J.L., 2004. Influence of non-glide stresses on plastic flow: from atomistic to continuum modeling. Materials Science and Engineering A 365, 31–37.

Wang, D., Pan, J., 2004. An anisotropic Gurson yield criterion for porous ductile sheet metals with planar anisotropy. International Journal of Damage Mechanics 13 (1), 7–33.